The Existence and Stability of Spike Equilibria in the One-Dimensional Gray-Scott Model: The Pulse-Splitting Regime

Theodore Kolokolnikov[*], Michael J. Ward[†], Juncheng Wei[‡]

Abstract

The existence, stability, and pulse-splitting behavior of spike patterns in the one-dimensional Gray-Scott model on a finite domain is analyzed in the semi-strong spike-interaction regime. This regime is characterized by a localization of one of the components of the reaction near certain spike locations, while the other component exhibits a more global spatial variation across the domain. The method of matched asymptotic expansions is used to construct k-spike equilibria in terms of a certain *core problem*. This core problem is studied numerically and qualitatively. For each integer $k > 1$, it is shown that there are two branches of k-spike equilibria that meet at a saddle-node bifurcation value. For small values of the diffusivity D of the second component, these saddle node bifurcation points occur at approximately the same value. A combination of asymptotic and numerical methods is used to analyze the stability of these branches of k-spike equilibria with respect to both drift instabilities associated with the small eigenvalues and oscillatory instabilities of the spike profile. In this way, the key bifurcation and spectral conditions of Ei, Nishiura, Ueda [Japan. J. Indus. Appl. Math., 18, (2001)] believed to be essential for pulse-splitting behavior in a reaction-diffusion system are verified. A simple analytical criterion for the occurrence of pulse-splitting is formulated and verified with full numerical simulations of the Gray-Scott model.

1 Introduction

We study the existence, stability, and pulse-splitting behavior of spike patterns in the one-dimensional Gray-Scott model. The Gray-Scott system, introduced in [15], models an irreversible reaction involving two reactants in a gel reactor, where the reactor is maintained in contact with a reservoir of one of

[*]Department of Mathematics, University of British Columbia, Vancouver, Canada V6T 1Z2
[†]Department of Mathematics, University of British Columbia, Vancouver, Canada V6T 1Z2, (corresponding author)
[‡]Department of Mathematics, Chinese University of Hong Kong, New Territories, Hong Kong

the two species in the reaction. This system can be written in nondimensional form as

$$V_T = D_v V_{XX} - (F+k)V + UV^2\,, \qquad 0 < X < L\,, \quad T > 0\,, \tag{1.1a}$$

$$U_T = D_u U_{XX} + F(1-U) - UV^2\,, \qquad 0 < X < L\,, \quad T > 0\,, \tag{1.1b}$$

$$U_X = V_X = 0\,, \qquad X = 0, L\,. \tag{1.1c}$$

Here $D_u > 0$, $D_v > 0$ are the constant diffusivities, $F > 0$ is the feed rate, and $k > 0$ is a reaction-time constant. For various ranges of these parameters, (1.1) and its two-dimensional counterpart, are known to posses a rich solution structure involving oscillating standing pulses, the propagation of traveling waves, pulse-replication behavior, and chaotic phenomena (cf. [5]–[9] [22], [23], [26]–[28], [30], [32], [33], [34], [35], [36], [37], and [38]).

We will analyze (1.1) in the singularly perturbed limit where D_v/D_u is asymptotically small. In our formulation, it is convenient to introduce the change of variables

$$v = V/\sqrt{F}\,, \qquad x = -1 + 2X/L\,, \qquad t = (F+k)T\,. \tag{1.2}$$

This leads to the dimensionless system

$$v_t = \varepsilon^2 v_{xx} - v + Auv^2\,, \qquad -1 < x < 1\,, \quad t > 0\,, \tag{1.3a}$$

$$\tau u_t = Du_{xx} + (1-u) - uv^2 \qquad -1 < x < 1\,, \quad t > 0\,, \tag{1.3b}$$

$$v_x(\pm 1, t) = u_x(\pm 1, t) = 0\,; \qquad v(x,0) = v_0(x)\,, \qquad u(x,0) = u_0(x)\,. \tag{1.3c}$$

Here $A > 0$, $D > 0$, $\tau > 1$, and $\varepsilon \ll 1$, are defined in terms of D_u, D_v, L, F, and k, by

$$D \equiv \frac{4D_u}{FL^2}\,, \qquad \varepsilon^2 \equiv \frac{4D_v}{L^2(F+k)}\,, \qquad \tau \equiv \frac{F+k}{F}\,, \qquad A \equiv \frac{\sqrt{F}}{F+k}\,. \tag{1.4}$$

The dimensionless system (1.3), first introduced in [28], is particularly convenient in that it shows that, for $\varepsilon \ll 1$, the construction of equilibrium solutions depends only on the two parameters A and D, while the reaction-time constant $\tau > 1$ only influences the stability of these solutions. Since $\varepsilon \ll 1$, for certain ranges of the parameters there are equilibrium solutions for v that consist of a sequence of spikes. The parameter D measures the effect of the finite domain and the strength of the inter-spike interactions. In this paper, we will assume that $D \gg O(\varepsilon^2)$ and $\varepsilon \ll 1$. In this regime, called the semi-strong spike interaction regime, spike patterns are such that v is localized near the spikes, while u varies more globally across the domain. This is to be contrasted with the weak spike interaction regime studied in [32], [33], and [38], where $D = O(\varepsilon^2)$ and $\varepsilon \ll 1$.

There are three regimes for A where different behaviors are found to occur. For the parameter range $A = O(\varepsilon^{1/2})$, referred to as the low feed-rate regime, there is a saddle-node bifurcation structure of equilibrium k-spike patterns, and the stability of these solutions depends intricately on A, D, and τ. This regime has been analyzed in detail in the companion paper [19]. For the intermediate regime, where $O(\varepsilon^{1/2}) \ll A \ll O(1)$, there are certain scaling laws in terms of a universal nonlocal eigenvalue problem that determine the stability of equilibrium spike patterns with respect to eigenvalues $\lambda = O(1)$ in the spectrum of the linearized problem. In this regime, studied in [7], [8], [9], [19], and [27], the finite domain and inter-spike coupling do not play a central role. In addition, in this regime and when τ is asymptotically large as $\varepsilon \to 0$, there can be drift instabilities associated with the small eigenvalues $\lambda = O(\varepsilon^2)$ in the spectrum of the linearization. These instabilities signify the birth of traveling wave solutions (see [26], [19]). In §2 we summarize the results of [19] for the intermediate regime that are relevant to the analysis in this paper. Finally, in the regime where $A = O(1)$, referred to here as the pulse-splitting regime, the equilibrium spike patterns again exhibit a saddle-node bifurcation structure, and this regime is intimately connected with a pulse-splitting behavior of spike patterns. For the infinite-line problem this was observed in [28], and also in [7] in terms of a different non-dimensionalization of the Gray-Scott model.

The goal of this paper is to analyze the existence and stability of spike patterns for (1.3) in the pulse-splitting regime where $A = O(1)$, $\varepsilon \ll 1$, and $D \gg O(\varepsilon^2)$. In §3 we construct equilibrium k-spike patterns in terms of a certain *core problem*. For the infinite-line problem, this core problem was introduced in [28]. We extend the analysis in [28] in two ways. Firstly, by allowing for a finite domain, and by matching the core solution to appropriate outer expansions, we show formally in Proposition 3.2 that when $A = O(1)$ and $\varepsilon A/\sqrt{D} \ll 1$, there are no k-spike equilibria to (1.3) that match smoothly onto the intermediate regime solutions when $A > A_{pk}$, where

$$A_{pk} \equiv 1.347 \coth\left(\frac{1}{k\sqrt{D}}\right) . \tag{1.5}$$

The value 1.347 arises from the saddle-node bifurcation value associated with the core problem (cf. [28]), while the other term in (1.5) arises from our analysis of (1.3) on the finite domain. Secondly, in §4 we investigate qualitative properties of the solutions to the core problem. The results are given in Propositions 4.1 and 4.2 below.

In §5 we study the stability of k-spike equilibria for $A = O(1)$ and $\varepsilon A/\sqrt{D} \ll 1$ with respect to drift instabilities associated with the small eigenvalues of order $\lambda = O(\varepsilon)$ in the spectrum of the linearization. In Proposition 5.2 we derive transcendental equations that the small eigenvalues satisfy. For $\tau \ll O(\varepsilon^{-1})$, in Proposition 5.3 we show that these eigenvalues are in the stable left half-plane for the equilibrium solution branch that merges onto the intermediate regime solution. In Propositions 5.4 and 5.5 we show that when $\tau = O(\varepsilon^{-1})$, and exceeds some critical value, a drift instability occurs as a result of a Hopf bifurcation. This leads to small-scale oscillations in the spike layer locations and a breathing-type instability (see Conjecture 5.6). A related type of Hopf bifurcation has been analyzed in [16] and [24] for hyperbolic tangent-type interfaces associated with a two-component reaction diffusion system with bistable nonlinearities. Related behavior for a three-component system has been shown numerically in [31]. In §6 we numerically study the stability of k-spike equilibria with respect to the large eigenvalues where $\lambda = O(1)$ as $\varepsilon \to 0$. For $\tau \ll O(\varepsilon^{-2})$, we show numerically that the equilibrium solution branch that merges onto the intermediate regime solutions is stable with respect to these eigenvalues, but that an instability due to a Hopf bifurcation in the spike profile can occur when τ is on the range $\tau = O(\varepsilon^{-2})$.

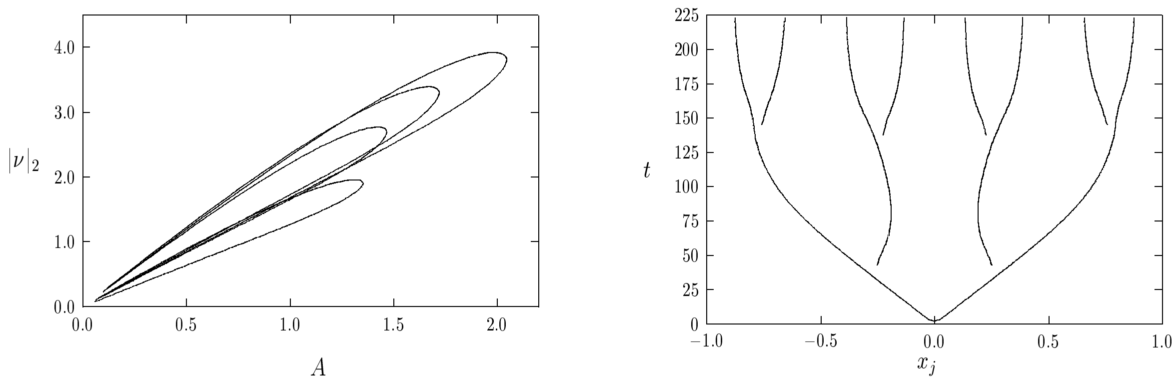

(a) $|\nu|_2$ versus A

(b) t versus x_j

Figure 1: Left figure: bifurcation diagram in the pulse-splitting regime $A = O(1)$ for k-spike solutions with $k = 1, \ldots, 4$. The fold point values for A increase with k. Right figure: trajectories of maxima of v illustrating pulse-splitting behavior when $\varepsilon = 0.01$, $D = 0.1$, $A = 2.4$, and $\tau = 2.0$.

In our pulse-splitting regime $A = O(1)$, with $\varepsilon A/\sqrt{D} \ll 1$, we show that the three pulse-splitting criteria of [10] are satisfied when $\tau \ll O(\varepsilon^{-1})$. The first condition of [10] is that each k-spike equilibrium branch on a suitable bifurcation diagram must have a fold-point, or saddle-node, bifurcation. Moreover, the fold points for each of these branches of equilibria must occur at approximately the same bifurcation value. This is the *lining-up property* of equilibria. In Fig. 1(a) we plot a bifurcation diagram of the norm of v versus A showing a saddle-node structure with an approximate lining-up property when $D = 0.1$. The saddle-node bifurcation values in this figure are the values A_{pk} given in (1.5). The second condition of [10] is that one of the branches of equilibria is unstable while the other is stable. When $\tau \ll O(\varepsilon^{-1})$ this stability condition is verified from the analysis and numerical computations in §5 and §6. The final condition is that the spectrum of the linearization of the equilibrium solution at the fold point location has a *dimple-shaped* eigenfunction Φ_d, associated with a zero eigenvalue, for one of the components of the system. Such an eigenfunction is computed numerically in §6. When the pulse-splitting conditions of [10] are satisfied, and when the bifurcation parameter is chosen to have a value slightly beyond the fold point value, pulse-splitting should occur from a single localized initial pulse. The *ghost* of the dimple eigenfunction at the fold point value still influences the system for values of the bifurcation parameter slightly beyond this critical value. Similar *ghost* effects in other bifurcation settings have been well-studied, including dynamical hysteresis loops (cf. [14]), and delayed bifurcation effects caused by slowly varying control parameters (cf. [12]).

From our analysis of the pulse-splitting regime, in §6 we then make a conjecture concerning the number of pulse-splitting events that will occur for (1.3) starting from a one-spike initial data. For $\tau \ll O(\varepsilon^{-1})$, $A = O(1)$, and $\varepsilon A/\sqrt{D} \ll 1$, Conjecture 6.1 predicts that a one-spike solution will undergo 2^{m-1} spitting events, and that the final equilibrium state will have 2^m spikes where, for some smallest integer $m > 0$, A lies in the interval

$$A_{p2^{m-1}} < A < A_{p2^m} \,. \tag{1.6}$$

Here A_{pk} is given in (1.5). In Fig. 1(b) we verify this conjecture for the case $\varepsilon = 0.01$, $D = 0.1$, $A = 2.4$, and $\tau = 2.0$. For these values we have $A_{p4} = 2.045$ and $A_{p8} = 3.583$, so that $A_{p4} < A < A_{p8}$. Therefore, the criterion (1.6) correctly predicts the eight-spike final state in Fig. 1(b).

An important remark is that in our analysis we require that $\varepsilon A/\sqrt{D} \ll 1$. Therefore, the pulse-splitting that occurs in our regime is *distinctly different* from the pulse-splitting that occurs in the parameter regime of [10], [32], [33], and [38], where $D = O(\varepsilon^2)$. When $D = O(\varepsilon^2)$, the inter-spike interactions become exponentially weak and there is a new core problem in the vicinity of each spike that involves a full balance of the terms in (1.3). In addition, pulse-splitting events occur only from the edge spikes (cf. [10]), in contrast to our regime where $\varepsilon A/\sqrt{D} \ll 1$ which involves a roughly simultaneous 2^m splitting of all the spikes in the sequence (see Fig. 1(b)).

In §7 we perform many numerical experiments to validate our asymptotic theory for pulse-splitting behavior, and we illustrate instabilities that can occur when τ is asymptotically large as $\varepsilon \to 0$. Finally, in §8 we make a few concluding remarks and we list some open problems.

2 The Intermediate Regime: $O(\varepsilon^{1/2}) \ll A \ll O(1)$

In this section, we summarize the main results of [19] for the existence and stability of k-spike equilibrium solutions to (1.3) in the intermediate regime where $O(\varepsilon^{1/2}) \ll A \ll O(1)$. Defining $\mathcal{A}$ by $A = \varepsilon^{1/2}\mathcal{A}$, we begin with the equilibrium result of [19] in the low feed-rate regime where $\mathcal{A} = O(1)$.

Proposition 2.1: *For $\varepsilon \to 0$, consider a k-spike equilibrium solution to (1.3) where the spikes have equal height. Then, when $\mathcal{A} > \mathcal{A}_{ke}$ there are two such solutions; the small solution u_-, v_-, and the large solution u_+, v_+. The v-component for such a solution satisfies*

$$v_\pm \sim \frac{1}{\sqrt{\varepsilon}\mathcal{A}U_\pm} \sum_{j=1}^{k} \left(w\left[\varepsilon^{-1}(x - x_j)\right] + O\left(\frac{\varepsilon}{\mathcal{A}^2 U_\pm^2 D}\right)\right) , \tag{2.1a}$$

where $w(y)$ satisfies (2.2) below and $x_j = -1 + (2j-1)/k$ for $j = 1, \ldots, k$. In the j^{th} inner region, where $|x - x_j| = O(\varepsilon)$, u is spatially constant to leading order, and satisfies

$$u_\pm \sim U_\pm \left[1 + O\left(\frac{\varepsilon}{\mathcal{A}^2 U_\pm^2 D}\right)\right] . \tag{2.1b}$$

Here $U_\pm$ and the saddle-node bifurcation value $\mathcal{A}_{ke}$ are given by

$$U_\pm = \frac{1}{2}\left[1 \pm \sqrt{1 - \frac{\mathcal{A}_{ke}^2}{\mathcal{A}^2}}\right] , \qquad \mathcal{A}_{ke} \equiv \sqrt{\frac{12\theta_0}{\tanh(\theta_0/k)}} , \qquad \theta_0 \equiv D^{-1/2} . \tag{2.1c}$$

The outer solution for u, valid for $|x - x_j| \gg O(\varepsilon)$ and $j = 1, \ldots, k$, is given by

$$u_\pm \sim 1 - \frac{(1 - U_\pm)}{a_g} \sum_{j=1}^{k} G(x; x_j) , \qquad a_g = \left[2\sqrt{D}\tanh(\theta_0/k)\right]^{-1} , \tag{2.1d}$$

where $G(x; x_j)$ is the Green's function satisfying (2.3) below.

This result was derived in Propositions 2.1 and 5.1 of [19]. In (2.1a), the profile $w(y)$ satisfies

$$w'' - w + w^2 = 0 , \qquad -\infty < y < \infty , \tag{2.2a}$$

$$w \to 0 \quad \text{as} \quad |y| \to \infty ; \qquad w'(0) = 0 , \quad w(0) > 0 . \tag{2.2b}$$

The solution is $w(y) = \frac{3}{2}\mathrm{sech}^2(y/2)$. In contrast, the u-component in (2.1d), which is the global variable, is determined in terms of the Green's function $G(x; x_j)$ satisfying

$$DG_{xx} - G = -\delta(x - x_j) , \qquad -1 < x < 1 ; \qquad G_x(\pm 1; x_j) = 0 . \tag{2.3}$$

In [19] the stability properties of (2.1) were examined in the low feed-rate regime $\mathcal{A} = O(1)$ (see §2–4 of [19]). Although the large solution v_+, u_+ was found to be unstable for any $\mathcal{A} > \mathcal{A}_{ke}$, the stability properties of the small solution v_-, u_- were found to depend intricately on the parameters D, τ, and k. Instabilities on an $O(1)$ time-scale were of two types: oscillatory instabilities arising from a Hopf bifurcation that occur when $\mathcal{A} > \mathcal{A}_{kL}$ and τ is sufficiently large, and competition instabilities arising from positive real eigenvalues that occur when $\mathcal{A}_{ke} < \mathcal{A} < \mathcal{A}_{kL}$ for any $\tau > 0$ (see §3 of [19]). For $\tau = O(1)$, it was shown in §4 of [19] that there are also slow drift instabilities that occur on a long time-scale of $O(\varepsilon^{-2})$ when $\mathcal{A}$ satisfies $\mathcal{A}_{ke} < \mathcal{A} < \mathcal{A}_{kS}$, where $\mathcal{A}_{kS} > \mathcal{A}_{kL}$. Precise formulae for the thresholds $\mathcal{A}_{kL}$ and $\mathcal{A}_{kS}$ were obtained in [19].

The stability properties of the small solution are much simpler in the intermediate regime where $O(1) \ll \mathcal{A} \ll O(\varepsilon^{-1/2})$, or equivalently when $O(\varepsilon^{1/2}) \ll \mathcal{A} \ll O(1)$ (see §5 of [19]). For the remainder of this section we re-label the small solution as v, u. For $\mathcal{A} \to \infty$, we get from (2.1c) that $U_- \sim \mathcal{A}_{ke}^2/4\mathcal{A}^2$. Substituting this relation into (2.1a) we obtain that v satisfies

$$v \sim \frac{\mathcal{A}\sqrt{D}}{3\sqrt{\varepsilon}\coth\left(\theta_0/k\right)} \sum_{j=1}^{k} \left(w\left[\varepsilon^{-1}(x-x_j)\right] + O\left(\frac{\varepsilon \mathcal{A}^2}{9\coth^2\left(\theta_0/k\right)}\right)\right) . \tag{2.4a}$$

In addition, the inner solution for u in (2.1b) becomes

$$u \sim \frac{3\coth\left(\theta_0/k\right)}{\mathcal{A}^2\sqrt{D}} \left[1 + O\left(\frac{\varepsilon \mathcal{A}^2}{9\coth^2\left(\theta_0/k\right)}\right)\right] . \tag{2.4b}$$

For $\mathcal{A} \gg 1$, the corresponding outer solution from (2.1d) becomes

$$u_0(x) \sim 1 - \frac{1}{a_g}\left(1 - \frac{\mathcal{A}_{ke}^2}{4\mathcal{A}^2}\right) \sum_{j=1}^{k} G(x;x_j) . \tag{2.4c}$$

To plot a bifurcation diagram, it is convenient to define a norm $|v|_2$ by

$$|v|_2 \equiv \left(\int_{-1}^{1} v^2\, dx \right)^{1/2} . \tag{2.5}$$

Then, in the intermediate regime, we obtain from (2.4a) that

$$|v|_2 \sim \frac{\sqrt{6Dk}\mathcal{A}}{3\coth\left(\theta_0/k\right)} . \tag{2.6}$$

In the intermediate parameter regime it was shown in Proposition 5.4 of [19] that a k-spike equilibrium solution is stable with respect to the drift instabilities associated with the small eigenvalues of order $\lambda = O(\varepsilon^2)$ when $D = O(1)$ and $\tau = O(1)$. Moreover, it was shown in [19] that there is a scaling law that determines the stability of the equilibrium solution with respect to the large $O(1)$ eigenvalues in the spectrum of the linearization. This latter result is summarized as follows:

Proposition 2.2: *Let $\varepsilon \ll 1$, $D = O(1)$, and $O(1) \ll \mathcal{A} \ll O(\varepsilon^{-1/2})$. Then, the k-spike equilibrium small solution u, v, is stable with respect to the large eigenvalues when $\tau < \tau_H$, where*

$$\tau_H \sim \frac{\mathcal{A}^4 D}{9} \tanh^4 (\theta_0/k)\, \tau_{0h} \left(1 - \frac{6\theta_0}{\mathcal{A}^2 \tanh(\theta_0/k)}\right)^2 + o(1)\,, \tag{2.7}$$

and $\tau_{0h} = 1.748$. As τ increases past τ_H, this solution loses its stability to a Hopf bifurcation.

This result was given in Proposition 5.3 of [19], and is based on spectral properties of the nonlocal eigenvalue problem

$$\Phi'' - \Phi + 2w\Phi - \frac{2w^2}{1+\sqrt{\tau_0 \lambda}} \left(\frac{\int_{-\infty}^{\infty} w\Phi\, dy}{\int_{-\infty}^{\infty} w\, dy} \right) = \lambda \Phi\,, \qquad -\infty < y < \infty\,, \tag{2.8}$$

with $\Phi \to 0$ as $|y| \to \infty$, where τ_0 is a bifurcation parameter.

The scaling law for τ given in (2.7) for a Hopf bifurcation of the spike profile shows that $\tau = O(\mathcal{A}^4) \gg 1$ when $\mathcal{A} \gg 1$. Therefore, it is natural to seek drift instabilities of a k-spike equilibrium solution that occur when $\tau \gg 1$. For a one-spike solution, this was done in §5.1 of [19], where the following result was obtained:

Proposition 2.3: *Let $\varepsilon \ll 1$ and $\tau = O(\varepsilon^{-2})$. Then, an eigenvalue $\lambda = O(\varepsilon^2)$ associated with a drift instability of the one-spike small equilibrium solution satisfies the nonlinear algebraic equation*

$$\lambda \sim \frac{2\varepsilon^2 s}{D} \left[\beta \tanh(\theta_0 \beta) \tanh \theta_0 - 1\right]\,, \qquad s \equiv \frac{1-U_-}{U_-}\,, \qquad \beta \equiv \sqrt{1+\tau\lambda}\,, \tag{2.9a}$$

where $\theta_0 = 1/\sqrt{D}$. In the intermediate parameter regime where $O(1) \ll \mathcal{A} \ll O(\varepsilon^{-1/2})$, (2.9a) reduces to

$$\lambda \sim \frac{2\varepsilon A^2}{3\sqrt{D}} \tanh\theta_0 \left[\beta \tanh(\theta_0 \beta) \tanh \theta_0 - 1\right]\,, \qquad \beta \equiv \sqrt{1+\tau\lambda}\,, \tag{2.9b}$$

where $A = \varepsilon^{1/2}\mathcal{A}$. For $\delta \ll 1$, any unstable mode associated with the one-spike solution has the form

$$v \sim \frac{1}{\sqrt{\varepsilon}\mathcal{A} U_-} w(\varepsilon^{-1}\left[x - x_0(t)\right])\,, \qquad x_0 \sim -\varepsilon \delta e^{\lambda t}\,. \tag{2.9c}$$

The results (2.9c) and (2.9a) were given in (5.37b) and (5.39) of [19], respectively. The limiting result (2.9b) is obtained by using the asymptotic relation $s \sim 4\varepsilon^{-1} A^2/\mathcal{A}_{1e}^2$ that holds in the intermediate regime. The analysis of (2.9a) was based on introducing the new variables τ_d, ω, and ξ, defined by

$$\tau = \left(\frac{D}{2s\varepsilon^2}\right)\tau_d\,, \qquad \lambda = \left(\frac{2s\varepsilon^2}{D}\right)\omega\,, \qquad \xi = \tau_d\omega\,. \tag{2.10}$$

Substituting (2.10) into (2.9a), it follows that ξ satisfies $F(\xi) = 0$, where

$$F(\xi) \equiv \frac{\xi}{\tau_d} - G(\xi)\,, \qquad G(\xi) \equiv \beta \tanh\theta_0 \tanh(\theta_0\beta) - 1\,, \qquad \beta \equiv \sqrt{1+\xi}\,. \tag{2.11}$$

By analyzing the roots of (2.11), the following result was obtained in Proposition 5.6 of [19]:

Proposition 2.4: *Let $\varepsilon \ll 1$ and $\tau = O(\varepsilon^{-2})$, and consider the small eigenvalues with $\lambda = O(\varepsilon^2)$. Then, there is a complex conjugate pair of pure imaginary eigenvalues when $\tau_d = \tau_{dh}$. For any $\tau_d > \tau_{dh}$ there are exactly two eigenvalues in the right half-plane. These eigenvalues have nonzero imaginary parts when $\tau_{dh} < \tau_d < \tau_{dm}$, and they merge onto the positive real axis at $\tau_d = \tau_{dm}$. They remain on the positive real axis for all $\tau_d > \tau_{dm}$. The values τ_{dh} and τ_{dm} depend on D.*

Therefore, at the critical value $\tau = \tau_{TW}$ given by

$$\tau_{TW} = \frac{D}{2s\varepsilon^2}\tau_{dh}\,, \tag{2.12}$$

a pair of complex small eigenvalues enters the right half-plane through a Hopf bifurcation. This instability with respect to translations in the spike profile leads to oscillations in the spike location, and is distinct from the Hopf bifurcation in the amplitude of the spike profile given in Proposition 2.2. By comparing the thresholds for τ given in (2.12) and (2.7), it follows that for $\varepsilon \ll 1$,

$$\tau_H \ll \tau_{TW}\,, \quad \text{for} \quad O(\varepsilon^{1/2}) \ll A \ll A_{sw}\,; \qquad \tau_{TW} \ll \tau_H\,, \quad \text{for} \quad A_{sw} \ll A \ll O(1)\,, \tag{2.13}$$

where $A_{sw} \sim \left(0.0047 D\tau_{dh}\coth^2\theta_0\right)^{1/6} \mathcal{A}_{1e}\varepsilon^{1/6}$.

Therefore, as A is increased towards the pulse-splitting regime where $A = O(1)$, a traveling wave instability will occur before the Hopf bifurcation value associated with the spike profile. Such an idea was given in [27] for a one-spike solution on the infinite line. Similar drift instabilities will occur in §5 when we analyze the pulse-splitting regime. Formally, if we set $\mathcal{A} = O(\varepsilon^{-1/2})$, or equivalently $A = O(1)$, in (2.12), (2.10), and (2.7), we can then use $s = O(\varepsilon^{-1})$ to suggest the following scalings for instabilities in the pulse-splitting regime where $A = O(1)$:

$$\tau_{TW} = O(\varepsilon^{-1})\,, \quad \lambda = O(\varepsilon)\,; \qquad \tau_H = O(\varepsilon^{-2})\,, \quad \lambda = O(1)\,. \tag{2.14}$$

3 Equilibria in the Pulse-Splitting Regime: $A = O(1)$

In this section we construct k-spike equilibria to (1.3) in the pulse-splitting regime where $A = O(1)$. To do so, we first construct a symmetric one-spike equilibrium solution to (1.3) on the interval $-l < x < l$. Then, by setting $l = 1/k$, we obtain the result for a k-spike pattern for (1.3) on $-1 < x < 1$.

The scalings for the inner region are suggested by (2.4). Therefore, in the inner region near $x = 0$, we let $y = \varepsilon^{-1}x$, $v_i(y) = v(\varepsilon y)$, $u_i(y) = u(\varepsilon y)$, and we expand the inner equilibrium solution for (1.3) on $-l < x < l$ as

$$v_i(y) = \varepsilon^{-1}\left(v_{i0} + \varepsilon v_{i1} + \cdots\right), \qquad u_i(y) = \varepsilon\left(u_{i0} + \varepsilon u_{i1} + \cdots\right). \tag{3.1}$$

We substitute (3.1) into (1.3), and collect powers of ε, to get inner problems on $-\infty < y < \infty$

$$v_{i0}'' - v_{i0} + A v_{i0}^2 u_{i0} = 0\,, \tag{3.2a}$$
$$D u_{i0}'' = u_{i0} v_{i0}^2\,, \tag{3.2b}$$
$$v_{i1}'' - v_{i1} + 2A v_{i0} u_{i0} v_{i1} = -A v_{i0}^2 u_{i1}\,, \tag{3.2c}$$
$$D u_{i1}'' = u_{i1} v_{i0}^2 + 2 u_{i0} v_{i0} v_{i1} - 1\,. \tag{3.2d}$$

We look for even solutions with $u_{i0}'(0) = v_{i0}'(0) = u_{i1}'(0) = v_{i1}'(0) = 0$. The far-field conditions as $y \to \infty$ are that v_{i0} and v_{i1} tend to zero exponentially, whereas the conditions for u_{i0} and u_{i1} will be obtained by matching.

To determine the effect of the inner solution on the outer problem for u, we calculate $\varepsilon^{-1}uv^2$ in the sense of distributions. In this way, we obtain that the outer solution u satisfies

$$D u_{xx} + (1 - u) = I_0 \delta(x) + \varepsilon I_1 \delta(x) + \cdots\,, \qquad -l < x < l\,, \tag{3.3a}$$

with $u_x(\pm l) = 0$, where $\delta(x)$ is the Dirac Delta function. Here I_0 and I_1 are defined by

$$I_0 \equiv \int_{-\infty}^{\infty} u_{i0} v_{i0}^2 \, dy\,, \qquad I_1 \equiv \int_{-\infty}^{\infty} \left(u_{i1} v_{i0}^2 + 2 v_{i0} v_{i1} u_{i0}\right) dy\,. \tag{3.3b}$$

Therefore, the solution to (3.3a) is

$$u(x) = 1 - I_0 G_l(x;0) - \varepsilon I_1 G_l(x;0) + \cdots\,. \tag{3.4}$$

Here $G_l(x;0)$ is the Green's function on $-l < x < l$ satisfying

$$D G_{lxx} - G_l = -\delta(x)\,, \quad -l < x < l\,; \qquad G_{lx}(\pm l;0) = 0\,. \tag{3.5}$$

A simple calculation gives,

$$G_l(x;0) = \left(\frac{\theta_0}{2}\right) \frac{\cosh\left[(l-|x|)\theta_0\right]}{\sinh(l\theta_0)} \,. \tag{3.6}$$

To determine the conditions for matching to the inner solution, we expand $u(x)$ in (3.4) as $x \to 0^{\pm}$. Using (3.6) to calculate $G_l(0;0)$, $G_{lx}(0^{\pm};0)$, and $G_{lxx}(0;0)$, we then set $x = \varepsilon y$ to get

$$u \sim 1 - \frac{\theta_0}{2} I_0 \coth(l\theta_0) \pm \frac{\varepsilon y \theta_0^2}{2} I_0 - \frac{\varepsilon\theta_0}{2} I_1 \coth(l\theta_0) - \frac{\varepsilon^2 y^2 \theta_0^3}{4} I_0 \coth(l\theta_0) \pm \frac{\varepsilon^2 \theta_0^2 y}{2} I_1 + O(\varepsilon^3) \,. \tag{3.7}$$

We now match (3.7) to the inner solution u_i given in (3.1). Since $u_i = O(\varepsilon)$, the $O(1)$ term in (3.7) must vanish. This yields,

$$I_0 = \int_{-\infty}^{\infty} u_{i0} v_{i0}^2 \, dy = \frac{2}{\theta_0 \coth(l\theta_0)} \,. \tag{3.8}$$

Then, the εy term in (3.7) determines the far-field behavior of u_{i0}. In this way, we obtain that v_{i0} and u_{i0} satisfy (3.2a) and (3.2b), subject to the far-field conditions

$$v_{i0} \to 0 \,, \qquad u_{i0} \sim \frac{\theta_0 |y|}{\coth(l\theta_0)} \,, \qquad \text{as} \quad |y| \to \infty \,. \tag{3.9}$$

It is convenient to introduce new variables V and U defined by

$$v_{i0} = \sqrt{D} V \,, \qquad u_{i0} = \frac{1}{A\sqrt{D}} U \,. \tag{3.10}$$

Substituting (3.10) into (3.2a), (3.2b), and (3.9), we obtain the leading-order problem, referred to as the **core problem**

$$V'' - V + V^2 U = 0 \,, \qquad 0 < y < \infty \,, \tag{3.11a}$$

$$U'' = UV^2 \,, \qquad 0 < y < \infty \,, \tag{3.11b}$$

$$V'(0) = U'(0) = 0 \,; \qquad V \to 0 \,, \qquad U \sim By \,, \qquad \text{as} \quad y \to \infty \,, \tag{3.11c}$$

where $U > 0$, $V > 0$, and

$$B \equiv \frac{A}{\coth(l\theta_0)} \,. \tag{3.12}$$

Before discussing some properties of this core problem, we continue with the matching to obtain a problem for the correction terms v_{i1} and u_{i1}. In terms of the solution to (3.11), there is a constant χ, depending on B, such that

$$U - By \to \chi \,, \qquad \text{as} \quad y \to \infty \,. \tag{3.13}$$

Then, the matching condition of the $O(\varepsilon)$ terms in the far-field behavior of the inner expansion for u and the outer expansion (3.7) determines I_1 in terms of χ by

$$I_1 = -\frac{2\chi}{A}\tanh(l\theta_0) = -\frac{2\chi}{B}\tanh^2(l\theta_0)\,. \tag{3.14}$$

Substituting (3.8) and (3.14) for I_0 and I_1, respectively, into the $O(\varepsilon^2)$ terms in the matching condition (3.7), we obtain that v_{i1} and u_{i1} satisfy (3.2c) and (3.2d), subject to the far-field conditions

$$v_{i1} \to 0\,, \qquad u_{i1} \sim -\frac{y^2}{2D} - \frac{\chi}{BD}\tanh^2(l\theta_0)y \qquad \text{as} \quad y \to \infty\,. \tag{3.15}$$

It is then convenient to introduce the new variables V_1 and U_1 defined by

$$v_{i1} = AV_1\,, \qquad u_{i1} = \frac{1}{D}U_1\,. \tag{3.16}$$

Substituting (3.16) into (3.2c), (3.2d), and (3.15), we obtain that the correction terms V_1, U_1 to the core solution satisfy

$$V_1'' - V_1 + 2VUV_1 = -V^2U_1\,, \qquad 0 < y < \infty\,, \tag{3.17a}$$

$$U_1'' = U_1V^2 + 2UVV_1 - 1\,, \qquad 0 < y < \infty\,, \tag{3.17b}$$

$$V_1'(0) = U_1'(0) = 0\,; \qquad V_1 \to 0\,, \qquad U_1 \sim -\frac{y^2}{2} - \frac{\chi}{B}\tanh^2(l\theta_0)y\,. \qquad \text{as} \quad y \to \infty\,. \tag{3.17c}$$

Here χ is defined by (3.13). Notice that U_1 is bounded uniformly in θ_0.

In summary, a two-term inner expansion is then obtained by substituting (3.10) and (3.16) into (3.1). This yields,

$$v_i = \frac{\sqrt{D}}{\varepsilon}\left[V + \frac{\varepsilon A}{\sqrt{D}}V_1 + \cdots\right], \qquad u_i = \frac{\varepsilon}{A\sqrt{D}}\left[U + \frac{\varepsilon A}{\sqrt{D}}U_1 + \cdots\right]. \tag{3.18}$$

Substituting I_0 and I_1 from (3.8) and (3.14) into (3.4), we obtain that the two-term outer expansion for u on $-l < x < l$ is

$$u(x) = 1 - \frac{G_l(x;0)}{G_l(0;0)} + \frac{2\varepsilon\chi}{B}\tanh^2(l\theta_0)G_l(x;0)\,, \tag{3.19}$$

where $G_l(x;0)$ is given in (3.6).

We now make a few remarks. Firstly, the error terms in (3.18) show that the inner expansion (3.18) is valid provided that

$$\frac{\varepsilon A}{\sqrt{D}} \ll 1\,. \tag{3.20}$$

Numerically, we will show below that the core problem (3.11) is closely connected to pulse-splitting behavior. This was certainly suggested in the analysis of [28] for a one-spike solution on the infinite line. Hence, our analysis of pulse-splitting in the semi-strong interaction regime will be valid provided that (3.20) holds. Notice that (3.20) is not valid for the other pulse-splitting regime $D = O(\varepsilon^2)$ studied numerically in [32], [33], and [38]. Hence, our analysis does not apply to this case. In this other pulse-splitting regime, where $A = O(1)$ and $D = O(\varepsilon^2)$, the inner solutions satisfy $v = O(1)$ and $u = O(1)$. Therefore, since all of the terms in (1.3) are important in the inner region, no asymptotic simplification is possible in the pulse-splitting regime $A = O(1)$ and $D = O(\varepsilon^2)$.

The second remark concerns the existence of asymmetric equilibrium patterns. Such patterns are possible when $u(l)$ is not monotone. However, a simple calculation using (3.19) and (3.6) shows that $u(l) = 1 - \operatorname{sech}(l\theta_0) + O(\varepsilon)$. Therefore, for $\varepsilon \ll 1$, $u(l)$ is monotone increasing, and so no asymmetric equilibria are possible.

To obtain a k-spike equilibrium solution we simply set $l = 1/k$, and extend $u(x)$ periodically across the interval from $-1 < x < 1$. This leads to our equilibrium result.

Proposition 3.1: *Let $\varepsilon \to 0$, $A = O(1)$, $\varepsilon A/\sqrt{D} \ll 1$, and suppose that the core problem (3.11) has a solution. Then, the v-component for a k-spike equilibrium solution to (1.3) is given by*

$$v \sim \frac{\sqrt{D}}{\varepsilon} \sum_{j=1}^{k} \left(V\left[\varepsilon^{-1}(x - x_j)\right] + \frac{\varepsilon A}{\sqrt{D}} V_1\left[\varepsilon^{-1}(x - x_j)\right] + \cdots \right) . \tag{3.21a}$$

In the j^{th} inner region, where $|x - x_j| = O(\varepsilon)$, u satisfies

$$u \sim \frac{\varepsilon}{A\sqrt{D}} \left(U\left[\varepsilon^{-1}(x - x_j)\right] + \frac{\varepsilon A}{\sqrt{D}} U_1\left[\varepsilon^{-1}(x - x_j)\right] + \cdots \right) . \tag{3.21b}$$

Here V, U satisfy (3.11), while V_1, U_1 satisfy (3.17). The outer solution for u, valid for $|x - x_j| \gg O(\varepsilon)$, and $j = 1, \ldots, k$, has the form

$$u \sim 1 - \frac{1}{a_g} \left(1 - \frac{\varepsilon \chi \theta_0}{B} \tanh\left(\frac{\theta_0}{k}\right) \right) \sum_{j=1}^{k} G(x; x_j) , \qquad a_g \equiv \frac{\theta_0}{2} \coth\left(\frac{\theta_0}{k}\right) . \tag{3.21c}$$

Here $G(x; x_j)$ is the Green's function, defined on $-1 < x < 1$, satisfying (2.3). The equilibrium spike locations are given by $x_j = -1 + (2j - 1)/k$ for $j = 1, \ldots, k$.

The norm $|v|_2$ in this region is obtained by substituting (3.21a) into (2.5) to get

$$|v|_2 \sim \varepsilon^{-1/2} \sqrt{kD} \left(\int_{-\infty}^{\infty} V^2 \, dy \right)^{1/2} . \tag{3.22}$$

3.1 The Core Problem

We now study the core problem (3.11) as a function of the parameter B. We first determine some analytical properties of (3.11). By integrating (3.11a) and (3.11b) from $0 < y < \infty$, and using (3.11c), we get

$$\int_0^\infty V^2 U \, dy = \int_0^\infty V \, dy = B \, . \tag{3.23}$$

To determine a good parameterization of the solution branch for (3.11), we define $U_0 \equiv U(0)$ and $V_0 \equiv V(0)$. Then, we multiply (3.11a) by V' and integrate the resulting equation from $0 < y < \infty$. Using (3.11c), we then obtain

$$\frac{V_0^2}{2} + \int_0^\infty \frac{U}{3} \left[V^3\right]' \, dy = \frac{V_0^2}{2} - \frac{U_0 V_0^3}{3} - \int_0^\infty \frac{1}{3} V^3 U' \, dy = 0 \, . \tag{3.24}$$

This gives,

$$\int_0^\infty V^3 U' \, dy = V_0^2 \left[\frac{3}{2} - U_0 V_0 \right] \, . \tag{3.25}$$

By integrating (3.11b) for U, and using $U'(0) = 0$, we obtain that $U' > 0$ on $0 < y < \infty$. Therefore, since the left hand-side of (3.25) is non-negative, we obtain a key inequality

$$0 < \gamma < \frac{3}{2} \, , \qquad \gamma \equiv U_0 V_0 \, . \tag{3.26}$$

As $\gamma \to 3/2$ from below, we show that there is a solution to (3.11) that has a single maximum for V and that matches onto the intermediate regime solution constructed in Proposition 2.1.

The inequality (3.26) provides a natural way to parameterize the solution branches of (3.11). Using the boundary value solver COLSYS [2], we compute the numerical solution to (3.11) as a function of $\gamma = U_0 V_0$ on the range $0 < \gamma < 3/2$. In the computations we started from a value of γ near $3/2$ and took as initial guess for the nonlinear solver the solution constructed in the intermediate regime in Proposition 2.1. In this way, we obtain a function $B = B(\gamma)$ from (3.11c). In Fig. 2(a) we show that $B(\gamma)$ is multi-valued with $B \to 0$ as $\gamma \to 0$ and as $\gamma \to 3/2$. Numerically, we find that the maximum value B_c of B and the point γ_c where this maximum occurs is

$$B_c = 1.347 \, , \qquad \gamma_c = 1.02 \, . \tag{3.27}$$

This value is consistent with that computed in [28] for the infinite-line problem. We refer to the upper branch in Fig. 2(a) as the *primary branch*, since it is this solution branch that merges smoothly as $B \to 0$ with the solution in the intermediate parameter regime. The lower branch in this figure is referred to as the *secondary branch*.

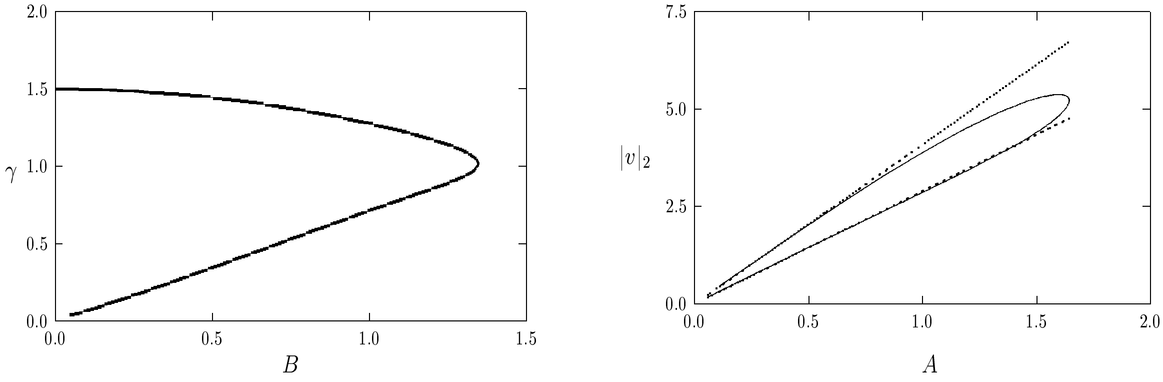

(a) γ versus B (b) $D = 0.75$

Figure 2: Left figure: plot of $\gamma = U_0 V_0$ versus B computed from the core problem (3.11). Right figure: plot of $|v|_2$ given in (3.22) (solid curve) versus A for a one-spike solution when $D = 0.75$ and $\varepsilon = 0.02$. The dashed curves are the limiting asymptotic results (4.13) and (4.25).

In Fig. 2(b) we plot the norm $|v|_2$, defined in (3.22), versus $A = B\coth(\theta_0)$ for a one-spike solution when $D = 0.75$ and $\varepsilon = 0.02$. The primary and secondary branches in the B, γ plane correspond to the upper and lower branches of Fig. 2(b), respectively. From (3.12) with $l = 1/k$, we can then make a formal proposition concerning the existence of k-spike equilibrium solutions to (1.3) in the pulse-splitting regime.

Proposition 3.2: *Let $\varepsilon \ll 1$, $A = O(1)$, and $\varepsilon A/\sqrt{D} \ll 1$. Then, there will be no k-spike equilibrium solution to (1.3) that merges onto the intermediate regime equilibrium solution when*

$$A > A_{pk} \equiv 1.347 \coth\left(\frac{1}{k\sqrt{D}}\right). \tag{3.28}$$

In Fig. 3(a) we plot the norm $|v|_2$, defined in (3.22), versus A for a k-spike solution with $k = 1, \ldots, 4$ when $\varepsilon = 0.02$ and $D = 0.75$. An identical plot is shown in Fig. 3(b) for the smaller value $D = 0.1$. Notice that for the smaller value of D there is an approximate lining-up property of k-spike equilibria. The primary branch again corresponds to the upper branches in these figures. The result (3.28) for the finite domain is new, and below it will provide a criterion for predicting the number of pulse-splitting events starting from initial data for (1.3).

In Fig. 4(a) we plot the numerical solution to (3.11) at the value $\gamma = 1.26$ where $B \approx 1.03$

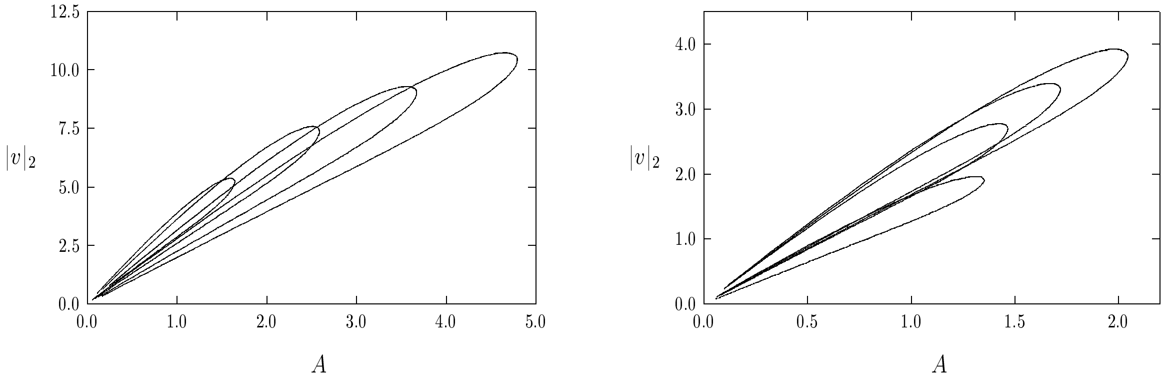

(a) $D = 0.75$

(b) $D = 0.1$

Figure 3: Left figure: plot of $|v|_2$ (solid curve) versus A for a k-spike solution with $k = 1, \ldots, 4$ when $\varepsilon = 0.02$ and $D = 0.75$. As k increases the value of A at the fold point increases. Right figure: same plot except that now $D = 0.1$. In this case, the fold points values are closer.

corresponding to a point on the primary branch. For the point $\gamma = 0.326$ where $B \approx 0.476$ on the secondary branch, a similar plot is shown in Fig. 4(b). Notice that this latter solution for v has two bumps. This feature is studied below in §4. Although a rigorous proof of the shape of the $B = B(\gamma)$ curve and the behavior of the solution to the core problem (3.11) appears to be difficult, in §4 we give some insight into the behavior of the solutions near the extreme portions of this curve, where either $\gamma \to 0$ or $\gamma \to 3/2$. In both of these limits $B \to 0$.

4 Asymptotics of the Core Problem

We now study the limiting behavior of the core problem (3.11). We first study the limiting behavior of the primary branch where $\gamma \to 3/2$ from below. In this limit we have that $U(0) \equiv U_0 \gg 1$, and so we introduce a small parameter δ by $\delta = 1/U_0$. This suggests that $U = O(\delta^{-1})$ and $V = O(\delta)$ in the core region. Therefore, in this limit, we expand the solution to (3.11) in terms of δ as

$$V = \delta \left(v_0 + \delta^2 v_1 + \cdots \right) , \qquad U = \delta^{-1} u = \delta^{-1} \left(u_0 + \delta^2 u_1 + \cdots \right) , \qquad \text{with} \quad u(0) = 1 . \tag{4.1}$$

Our choice of δ enforces that $u_0(0) = 1$ and $u_j(0) = 0$ for $j \geq 1$. Since $\int_0^\infty V \, dy = B$ from (3.23), the expansion (4.1) yields that $B = O(\delta)$. Hence, we write $B = \delta B_0$. Substituting (4.1) into (3.11), and

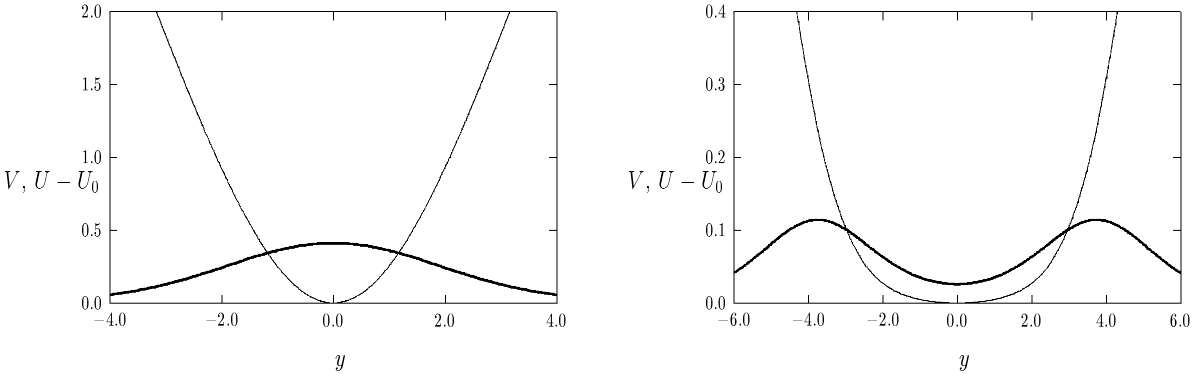

(a) Primary branch: $\gamma = 1.263$, $B \approx 1.03$ (b) Secondary branch: $\gamma = 0.326$, $B \approx 0.476$

Figure 4: Plots of the numerical solution to the core problem on either side of the fold point at $B = B_c = 1.347$ and $\gamma = \gamma_c = 1.02$. The heavy solid curves are V, while the solid curves are $U - U_0$.

collecting powers of δ, we obtain the leading-order problem

$$v_0'' - v_0 + v_0^2 u_0 = 0\,, \qquad u_0'' = 0\,, \tag{4.2}$$

with $v_0'(0) = 0$, $u_0(0) = 1$, $v_0 \to 0$ as $y \to \infty$, and $u_0' \to 0$ as $y \to \infty$. Therefore, we get $u_0(y) = 1$ and $v_0(y) = w(y)$, where w satisfies (2.2). From collecting terms of order $O(\delta^2)$, we obtain that v_1 and u_1 satisfy

$$Lv_1 \equiv v_1'' - v_1 + 2wv_1 = -w^2 u_1\,, \quad 0 < y < \infty\,; \qquad v_1'(0) = 0\,, \quad v_1 \to 0\,, \quad \text{as} \quad y \to \infty\,, \tag{4.3a}$$

$$u_1'' = w^2\,, \quad 0 < y < \infty\,; \qquad u_1'(0) = 0\,, \quad u_1(0) = 0\,, \quad u_1' \to B_0\,, \quad \text{as} \quad y \to \infty\,. \tag{4.3b}$$

By integrating (4.3b) over $0 < y < \infty$, we get that $B_0 = \int_0^\infty w^2\, dy = 3$.

Next, we multiply (4.3a) by w' and integrate over $0 < y < \infty$. Then, using $Lw' = 0$ and $w'(0) = v_1'(0) = 0$, we get

$$\int_0^\infty w' Lv_1\, dy = w''(0) v_1(0) = -\int_0^\infty w^2 w' u_1\, dy\,. \tag{4.4}$$

Integrating the last term in (4.4) by parts, and noting that $u_1(0) = 0$, we get

$$w''(0) v_1(0) = \frac{1}{3} \int_0^\infty w^3 u_1'\, dy\,. \tag{4.5}$$

To calculate $v_1(0)$, we must determine $u_1^{'}(y)$. To do so, we substitute $w(y) = \frac{3}{2}\text{sech}^2\,(y/2)$ and $w^2 = w - w^{''}$ directly into (4.3b) to get

$$u_1^{''} = w - w^{''} = \frac{3}{2}\text{sech}^2\,(y/2) - w^{''}\,. \tag{4.6}$$

Integrating this equation twice, and using $u_1^{'}(0) = 0$, $u_1(0) = 0$, we readily obtain

$$u_1(y) = 6\ln\left[\cosh\left(\frac{y}{2}\right)\right] - \frac{3}{2}\text{sech}^2\left(\frac{y}{2}\right) + \frac{3}{2}\,. \tag{4.7}$$

To determine $v_1(0)$, we integrate (4.6) once to get

$$u_1^{'} = 3\tanh\left(\frac{y}{2}\right) - w^{'} = -\frac{3w^{'}}{w} - w^{'}\,. \tag{4.8}$$

Finally, substituting (4.8) into (4.5), integrating the resulting expression by parts, and using the explicit form of w, we obtain

$$v_1(0) = \frac{1}{3w''(0)}\int_0^\infty \left(-3w^2 w^{'} - w^{'}w^3\right)\,dy = \frac{1}{3w''(0)}\left[w^3(0) + \frac{w^4(0)}{4}\right] = -\frac{33}{16}\,. \tag{4.9}$$

Since $\gamma \equiv U_0V_0$, we use (4.1) to get $\gamma = w(0) + \delta^2 v_1(0)$. We summarize the result of this calculation in the following formal proposition:

Proposition 4.1: *Let $\delta = 1/U_0 \ll 1$. Then, along the primary branch, the core problem (3.11) has a solution where $\gamma \to 3/2$ from below as $\delta \to 0$. This solution is given asymptotically by*

$$V \sim \delta\left(w(y) + \delta^2 v_1(y) + \cdots\right)\,, \qquad U \sim \delta^{-1}\left(1 + \delta^2 u_1(y) + \cdots\right)\,, \tag{4.10a}$$

where $w(y)$ satisfies (2.2). Here $u_1(y)$ is given in (4.7), and

$$B = 3\delta + \cdots\,, \qquad \gamma \equiv U_0V_0 = \frac{3}{2} - \frac{33}{16}\delta^2 + \cdots\,. \tag{4.10b}$$

This gives the following local behavior for the $B = B(\gamma)$ curve:

$$\gamma \equiv U_0V_0 \sim \frac{3}{2} - \frac{11B^2}{48}\,, \qquad \text{as} \quad B \to 0\,. \tag{4.10c}$$

We now show that this limiting solution makes a smooth transition to the intermediate regime inner solution constructed in Proposition 2.1 of §2. To show this, we use $B = 3\delta$ and (3.12) to calculate δ in terms of A for a k-spike solution as

$$A = 3\delta\coth\left(\frac{\theta_0}{k}\right)\,. \tag{4.11}$$

Substituting the leading terms of (4.10a) into the leading terms of (3.18), we obtain for $\delta \ll 1$, that

$$v_i \sim \frac{A\sqrt{D}w}{3\varepsilon \coth(\theta_0/k)}, \qquad u_i \sim \frac{3\varepsilon \coth(\theta_0/k)}{A^2\sqrt{D}}. \tag{4.12}$$

This expression reproduces the leading-order terms in the intermediate regime inner expansion given in Proposition 2.1. Moreover, for $\delta \ll 1$, we can use $V \sim \delta w$, to calculate the norm in (3.22) as

$$|v|_2 \sim \varepsilon^{-1/2}\sqrt{kD}\left(\int_{-\infty}^{\infty} V^2\, dy\right)^{1/2} \sim \frac{A\varepsilon^{-1/2}\sqrt{6kD}}{3\coth(\theta_0/k)}. \tag{4.13}$$

This result agrees asymptotically with the intermediate regime norm given in (2.6). Therefore, the limiting behavior of the primary branch where $U_0V_0 \to 3/2$ from below provides a smooth transition to the expansions in the intermediate regime constructed in §5.

For the secondary solution branch in the B, γ parameter plane, we now construct an asymptotic solution to the core problem (3.11) where $\gamma \equiv U_0V_0 \to 0$ from above. From (3.11a), we first observe that $V''(0) < 0$ when $\gamma > 1$, and $V''(0) > 0$ when $0 < \gamma < 1$. Therefore, for values of γ just below $\gamma = 1$, the solution for V starts to have a dimple at the origin. As γ is decreased further, this dimple becomes more pronounced, and as $\gamma \to 0$ the solution to (3.11) begins to look like two spikes symmetrically placed about the origin. This was illustrated in Fig. 4(b) for $\gamma = 0.326$ where $B \approx 0.476$. It is remarkable that the fold point value $\gamma_c = 1.02$, given in (3.27), occurs at almost the same value as where V first begins to exhibit a dimple. Therefore, as $\gamma = U_0V_0 \to 0$, we expect that the core solution splits into two disjoint spikes.

To analyze this regime, we again label $\delta = 1/U_0$, with $U_0 \equiv U(0)$, except that now we make a two-spike approximation for V with spikes located at $y = y_1 > 0$ and $y = -y_1$. As $\delta \to 0$, we will show that $y_1 \sim -\ln\delta \gg 1$. Therefore, the separation between the spikes grows as δ decreases. The analysis below to calculate y_1 is similar in essence to the analytical construction of multi-bump solutions to the Gierer-Meinhardt model (cf. [13]) given in [4].

We look for a two-bump solution to (3.11) in the form

$$V = \delta\left(w_1 + w_2 + R + \cdots\right), \qquad U = \delta^{-1}u = \delta^{-1}\left(1 + \delta^2 u_1 + \cdots\right), \qquad \text{with} \quad u_1(0) = 0. \tag{4.14}$$

Here we have labelled $w_1(y) \equiv w(y - y_1)$ and $w_2(y) \equiv w(y + y_1)$. Substituting (4.14) into (3.11), and assuming that $R \ll 1$, we obtain that u_1 and the residual R satisfy

$$LR \equiv R'' - R + 2(w_1 + w_2)R = -2w_1w_2 - \delta^2\left(w_1^2 + w_2^2 + 2w_1w_2\right)u_1, \quad -\infty < y < \infty, \tag{4.15a}$$

$$u_1'' = w_1^2 + w_2^2 + 2w_1w_2, \qquad -\infty < y < \infty, \tag{4.15b}$$

with $u_1'(0) = 0$. Notice that R is small when the bumps are widely separated. In particular, when $y_1 = O(-\ln\delta)$, the two terms on the right hand-side of (4.15a) are both of order $O(\delta^2)$.

To determine y_1 we use a solvability condition. Assuming that the spikes are well-separated so that $y_1 \gg 1$, we multiply (4.15a) by w_1', and then integrate by parts over $-\infty < y < \infty$ to obtain the solvability condition

$$0 = \int_{-\infty}^{\infty} w_1' LR \, dy \sim -2\int_{-\infty}^{\infty} w_1 w_1' w_2 \, dy - \delta^2 \int_{-\infty}^{\infty} w_1^2 w_1' u_1 \, dy \,. \tag{4.16}$$

The dominant contribution to the first integral on the right hand-side of (4.16) arises from the region where $y = y_1$. In this region, we use $w(y) \sim 6e^{-y}$ to get $w(y+2y_1) \sim 6e^{-y-2y_1}$. In this way, we calculate

$$I_1 \equiv 2\int_{-\infty}^{\infty} w_1 w_1' w_2 \, dy \sim 2\int_{-\infty}^{\infty} w(y) w'(y) w(y+2y_1) \, dy \sim 12 e^{-2y_1} \int_{-\infty}^{\infty} e^{-y} w(y) w'(y) \, dy \,. \tag{4.17}$$

Integrating the last expression in (4.17) by parts, and then using $w^2 = w - w''$, we obtain

$$I_1 \sim 6e^{-2y_1} \int_{-\infty}^{\infty} e^{-y} \left(w - w'' \right) \, dy = 6e^{-2y_1} \lim_{y \to -\infty} \left[e^{-y} \left(w + w' \right) \right] = 72 e^{-2y_1} \,. \tag{4.18}$$

To calculate the other integral on the right hand-side of (4.16) we integrate by parts once and use $u_1(0) = 0$ to get

$$I_2 \equiv \delta^2 \int_{-\infty}^{\infty} w_1^2 w_1' u_1 \, dy = -\frac{\delta^2}{3} \int_{-\infty}^{\infty} w_1^3 u_1' \, dy = -\frac{\delta^2}{3} \int_{-\infty}^{\infty} [w(y)]^3 \, u_1'(y+y_1) \, dy \,. \tag{4.19}$$

Next, by integrating (4.15b) with $u_1'(0) = 0$, we get

$$u_1'(y) \sim \int_0^y [w(s-y_1)]^2 \, ds \,. \tag{4.20}$$

We can then write $u_1'(y+y_1)$ as

$$u_1'(y+y_1) \sim \int_{-y_1}^{0} [w(s)]^2 \, ds + \int_0^y [w(s)]^2 \, ds \sim 3 + \int_0^y [w(s)]^2 \, ds \,. \tag{4.21}$$

Here we have used $\int_{-y_1}^0 w^2 \, dy \sim \int_{-\infty}^0 w^2 \, dy = 3$ for $y_1 \gg 1$. The integral on the right hand-side of (4.21) is odd. Therefore, upon substituting (4.21) into (4.19), we get an integral that is readily evaluated as

$$I_2 \sim -\delta^2 \int_{-\infty}^{\infty} [w(y)]^3 \, dy = -\frac{36\delta^2}{5} \,. \tag{4.22}$$

Finally, substituting (4.22) and (4.18) into (4.16), we obtain that y_1 satisfies

$$72e^{-2y_1} \sim \frac{36\delta^2}{5} \,. \tag{4.23}$$

The product $\gamma \equiv U_0 V_0$ is calculated as $\gamma \sim [w_1(0) + w_2(0)] = 2w(y_1)$. Since $y_1 \gg 1$, we use $w(y) \sim 6e^{-y}$ to get $\gamma \sim 12e^{-y_1}$, where y_1 satisfies (4.23). Finally, B is determined by $B = \delta \int_0^\infty \left[w_1^2 + w_2^2\right] \, dy \sim 6\delta$. This formal construction of a two-bump solution is summarized as follows:

Proposition 4.2: *Let $\delta = 1/U_0 \ll 1$. Then, along the secondary branch, the core problem (3.11) has a solution where $\gamma \equiv U_0 V_0 \to 0$ from above as $\delta \to 0$. This solution is given asymptotically by*

$$V \sim \delta \left[w(y - y_1) + w(y + y_1)\right] \qquad U \sim \frac{1}{\delta} \left(1 + \delta^2 \left[u_1(y - y_1) + u_1(y + y_1) - 2u(y_1)\right]\right) \,, \tag{4.24a}$$

where $w(y)$ satisfies (2.2), and $u_1(y)$ is given explicitly in (4.7). The constants $\gamma \equiv U_0 V_0$, y_1, and B, are given for $\delta \ll 1$ by

$$B = 6\delta + \cdots \,, \qquad \gamma \equiv U_0 V_0 \sim \frac{6\delta\sqrt{2}}{\sqrt{5}} \,, \qquad y_1 \sim -\ln\delta + \frac{1}{2}\ln 10 \,. \tag{4.24b}$$

This implies the following local behavior for the $B = B(\gamma)$ curve:

$$\gamma \equiv U_0 V_0 \sim \sqrt{2}B/\sqrt{5} \,, \qquad \text{as} \quad B \to 0 \,. \tag{4.24c}$$

In this limit, we can also calculate the limiting form of the norm defined in (3.22). Substituting the inner expansion for v from (4.24a) into (3.22), and using $\delta = B/6$ and $B = A/\coth(l\theta_0)$, we obtain

$$|v|_2 \sim \varepsilon^{-1/2}\sqrt{kD} \left(\int_{-\infty}^{\infty} V^2 \, dy\right)^{1/2} \sim \frac{A\varepsilon^{-1/2}\sqrt{12kD}}{6\coth(\theta_0/k)} \,. \tag{4.25}$$

This analysis shows that on the secondary branch a one-spike equilibrium solution splits into a two-spike solution where the spikes are separated by an amount of order $O(-\ln B)$ as $B \to 0$. This analysis is new and is closely related to the pulse-splitting behavior computed below.

The results in Propositions 4.1 and 4.2 were partially validated in Fig. 2(b), where we plotted the asymptotic results (4.13) and (4.25) to the norm $|v|_2$ that are valid at the two extremities of the $B = B(\gamma)$ curve. From this figure, these asymptotic approximations are rather good over most of the curve. In Fig. 5(a) we compare the two asymptotic results $\gamma \sim \frac{3}{2} - 11B^2/48$ and $\gamma \sim \sqrt{2}B/\sqrt{5}$ as $B \to 0$, obtained from Propositions 4.1 and 4.2, with the numerically computed curve $B = B(\gamma)$. Except near the fold point, these results are rather good. Finally, in Fig. 5(b) we plot the numerically computed U_0 versus γ together with the asymptotic results of Propositions 4.1 and 4.2.

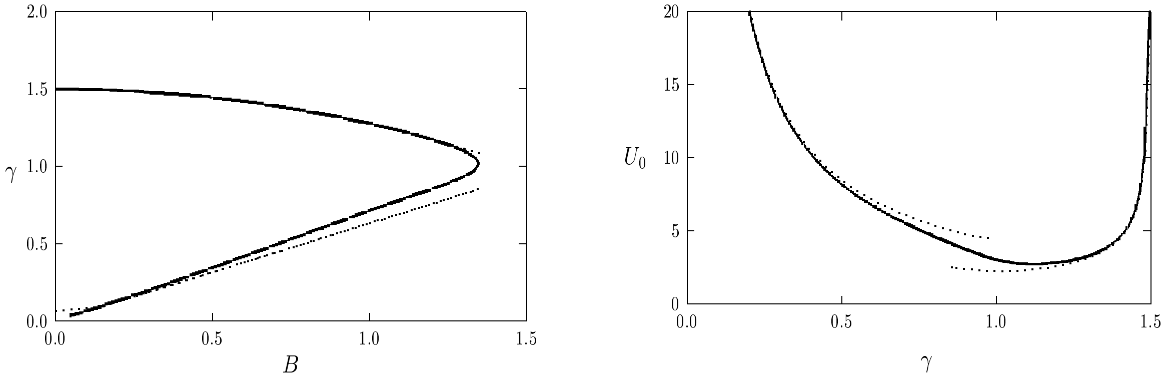

(a) $\gamma = U_0 V_0$ versus B

(b) U_0 versus $\gamma = U_0 V_0$

Figure 5: Numerical (solid curves) and asymptotic approximations (dashed curves) obtained from Propositions 4.1 and 4.2. Left figure: $\gamma = U_0 V_0$ versus B. Right figure: U_0 versus γ.

5 Drift Instabilities: The Small Eigenvalues

In this section we extend the results in Propositions 2.3 and 2.4 in the intermediate parameter regime by looking for drift instabilities associated with the k-spike equilibrium solution constructed in Proposition 3.1.

We begin by linearizing (1.3) around the equilibrium solution constructed above in Proposition 3.1. Let v_e and u_e denote this equilibrium solution. We write

$$v = v_e + e^{\lambda t}\phi\,, \qquad u = u_e + e^{\lambda t}\eta\,. \tag{5.1}$$

Substituting (5.1) into (1.3) we obtain the eigenvalue problem

$$\varepsilon^2\phi_{xx} - \phi + 2Au_e v_e \phi + A\eta v_e^2 = \lambda\phi\,, \qquad -1 < x < 1\,, \tag{5.2a}$$

$$D\eta_{xx} - \eta - \eta v_e^2 - 2u_e v_e \phi = \tau\lambda\eta\,, \qquad -1 < x < 1\,. \tag{5.2b}$$

We begin by examining (5.2) in the j^{th} inner region where $y = \varepsilon^{-1}(x - x_j)$. Using (3.21a) and (3.21b), we calculate

$$2Au_e v_e \sim 2\left[UV + \frac{\varepsilon A}{\sqrt{D}}\left(UV_1 + U_1 V\right) + \cdots\right], \qquad v_e^2 \sim \frac{D}{\varepsilon^2}\left[V^2 + \frac{2\varepsilon A}{\sqrt{D}}VV_1 + \cdots\right], \tag{5.3}$$

where U, V satisfy (3.11), and U_1, V_1 satisfy (3.17). In this inner region we introduce Φ and N by

$$\phi(x) = \frac{A}{\varepsilon}\Phi\left(y;\varepsilon\right) \,, \qquad \eta(x) = \frac{\varepsilon}{D}N\left(y;\varepsilon\right) \,. \tag{5.4}$$

Substituting (5.4) and (5.3) into (5.2), and with $y = \varepsilon^{-1}(x - x_j)$, we obtain the following inner problem on $-\infty < y < \infty$:

$$\Phi_{yy} - \Phi + 2\left[UV + \frac{\varepsilon A}{\sqrt{D}}\left(UV_1 + U_1V\right) + \cdots\right]\Phi + \left[V^2 + \frac{2\varepsilon A}{\sqrt{D}}VV_1 + \cdots\right]N = \lambda\Phi \,, \tag{5.5a}$$

$$N_{yy} - \left[V^2 + \frac{2\varepsilon A}{\sqrt{D}}VV_1 + \cdots\right]N - 2\left[UV + \frac{\varepsilon A}{\sqrt{D}}\left(UV_1 + U_1V\right) + \cdots\right]\Phi = \frac{\varepsilon^2}{D}(1+\tau\lambda)N \,. \tag{5.5b}$$

As suggested by the intermediate regime result (2.14), we look for instabilities associated with small eigenvalues of order $\lambda = O(\varepsilon)$. Therefore, we seek an eigenfunction to (5.5) in the form

$$\Phi(y;\varepsilon) = \Phi_0(y) + \frac{\varepsilon A}{\sqrt{D}}\Phi_1(y) + \cdots \,, \qquad N(y;\varepsilon) = N_0(y) + \frac{\varepsilon A}{\sqrt{D}}N_1(y) + \cdots \,, \qquad \lambda = \frac{\varepsilon A}{\sqrt{D}}\lambda_0 + \cdots \,. \tag{5.6}$$

Substituting (5.6) into (5.5), we collect the leading-order terms to get

$$\Phi_{0yy} - \Phi_0 + 2UV\Phi_0 + V^2N_0 = 0 \,, \quad -\infty < y < \infty \,, \tag{5.7a}$$

$$N_{0yy} - V^2N_0 - 2UV\Phi_0 = 0 \,, \quad -\infty < y < \infty \,. \tag{5.7b}$$

We look for an odd eigenfunction of (5.7) with $\Phi_0 \to 0$ and N_0 bounded as $|y| \to \infty$. From the $O(\varepsilon)$ terms, we get the system for the next order correction

$$\Phi_{1yy} + (-1 + 2UV)\Phi_1 + V^2N_1 = \lambda_0\Phi_0 - 2(UV_1 + U_1V)\Phi_0 - 2VV_1N_0 \,, \quad -\infty < y < \infty \,, \tag{5.8a}$$

$$N_{1yy} - 2UV\Phi_1 - V^2N_1 = 2(UV_1 + U_1V)\Phi_0 + 2VV_1N_0 \,, \quad -\infty < y < \infty \,. \tag{5.8b}$$

By differentiating (3.11), it is clear that a solution to (5.7) is

$$\Phi_0 = c_jV_y \,, \qquad N_0 = c_jU_y \,. \tag{5.9}$$

This solution is odd, and we assume that this is the only solution to (5.7). The constant c_j, associated with this j^{th} inner region, will be determined below after matching to the outer solution. Substituting (5.9) into (5.8), we then express (5.8) in matrix form as

$$\mathcal{L}\Psi = c_j\begin{pmatrix} \lambda_0 & 0 \\ 0 & 0 \end{pmatrix}\begin{pmatrix} V_y \\ U_y \end{pmatrix} + c_j\begin{pmatrix} -2(UV_1 + U_1V) & -2VV_1 \\ 2(UV_1 + U_1V) & 2VV_1 \end{pmatrix}\begin{pmatrix} V_y \\ U_y \end{pmatrix} \,, \tag{5.10a}$$

where $\Psi \equiv (\Phi_1, N_1)^t$, and the operator $\mathcal{L}$ is defined by

$$\mathcal{L}\Psi \equiv \begin{pmatrix} \Phi_{1yy} \\ N_{1yy} \end{pmatrix} + E \begin{pmatrix} \Phi_1 \\ N_1 \end{pmatrix}, \qquad E \equiv \begin{pmatrix} -1+2UV & V^2 \\ -2UV & -V^2 \end{pmatrix}. \tag{5.10b}$$

We look for an odd solution to (5.10a) where $\Phi_1 \to 0$ as $|y| \to \infty$. As shown below upon matching to the outer region, the appropriate boundary condition for N_1 is that N_{1y} is bounded as $|y| \to \infty$. To determine the solvability condition for (5.10), we let $\Psi^\dagger$ denote the solution of the homogeneous adjoint equation

$$\mathcal{L}^\dagger \Psi^\dagger \equiv \begin{pmatrix} \Psi^\dagger_{1yy} \\ \Psi^\dagger_{2yy} \end{pmatrix} + E^t \begin{pmatrix} \Psi^\dagger_1 \\ \Psi^\dagger_2 \end{pmatrix} = 0\,, \tag{5.11}$$

where t denotes transpose. We look for an odd solution to (5.11) where $\Psi^\dagger_1 \to 0$ and $\Psi^\dagger_{2y} \to 0$ as $|y| \to \infty$.

To determine the solvability condition for (5.10a), we multiply (5.10a) by $\Psi^{\dagger t}$ and integrate by parts to get

$$\int_{-\infty}^{\infty} \Psi^{\dagger t} \mathcal{L}\Psi \, dy = \left(\Psi^{\dagger t} \Psi_y - \Psi^t \Psi^\dagger_y \right) |_{-\infty}^{\infty} = c_j \lambda_0 I_2 + c_j I_1\,, \tag{5.12a}$$

where I_1 and I_2 are defined by

$$I_1 \equiv \int_{-\infty}^{\infty} \left(\Psi_2^{\dagger t} - \Psi_1^{\dagger t} \right) \left[2(UV)_y V_1 + (V^2)_y U_1 \right] \, dy\,, \qquad I_2 \equiv \int_{-\infty}^{\infty} \Psi^\dagger_1 V_y \, dy\,. \tag{5.12b}$$

Since Ψ and $\Psi^\dagger$ are odd functions and $\Psi^\dagger_y \to 0$ as $y \to \infty$, (5.12a) can be reduced to

$$c_j \lambda_0 I_2 = -c_j I_1 + 2\Psi^\dagger_2(\infty) N_{1y}(\infty)\,. \tag{5.12c}$$

The next step in the analysis is to calculate I_1 explicitly. To do so, we introduce W by $W = (V_{1y}, U_{1y})^t$. Upon differentiating the system (3.17) for V_1 and U_1 with respect to y, it follows that

$$\mathcal{L}W = \begin{pmatrix} -2(UV)_y V_1 - (V^2)_y U_1 \\ 2(UV)_y V_1 + (V^2)_y U_1 \end{pmatrix}. \tag{5.13}$$

Therefore, I_1 in (5.12b) can be written in terms of W. Integrating the resulting expression by parts, we get

$$I_1 = \int_{-\infty}^{\infty} \Psi^{\dagger t} \mathcal{L}W \, dy = \left(\Psi^{\dagger t} W_y - \Psi_y^{\dagger t} W \right) |_{-\infty}^{\infty} + \int_{-\infty}^{\infty} W^t \mathcal{L}^\dagger \Psi^\dagger \, dy\,. \tag{5.14}$$

Using $\mathcal{L}^\dagger \Psi^\dagger = 0$, with $\Psi^\dagger_1 \to 0$ and $\Psi^\dagger_{2y} \to 0$ as $|y| \to \infty$, (5.14) reduces to

$$I_1 = 2\Psi^\dagger_2(\infty) U_{1yy}(\infty) = -2\Psi^\dagger_2(\infty)\,. \tag{5.15}$$

Here we have used $U_{1yy}(\infty) = -1$ as seen from (3.17c). Finally, substituting (5.15) into (5.12c), we obtain a compact expression for λ_0

$$c_j \lambda_0 \int_{-\infty}^{\infty} \Psi_1^\dagger V_y \, dy = 2\Psi_2^\dagger(\infty) \left[N_{1y}(\infty) + c_j \right] , \qquad j = 1, \ldots, k . \tag{5.16}$$

This completes the analysis of the j^{th} inner region.

Next, we match this j^{th} inner solution constructed above to the outer solution for (5.2). This will determine $N_{1y}(\infty)$ and the constants c_j, for $j = 1, \ldots, k$. In the outer region, away from $O(\varepsilon)$ regions centered at the spike equilibrium locations, ϕ in (5.2a) is exponentially small and η in (5.2b) is given by

$$D\eta_{xx} - (1 + \tau\lambda)\eta = \eta v_e^2 + 2u_e v_e \phi . \tag{5.17}$$

Since the right hand-side of (5.17) is localized near each $x = x_j$ for $j = 1, \ldots, k$, its effect on the outer solution can be calculated in the sense of distributions. Recalling (5.4), (5.6), and (3.21), we get $\phi \sim A c_j \varepsilon^{-1} V_y$, $\eta \sim \varepsilon c_j D^{-1} U_y$, $v_e^2 \sim D\varepsilon^{-2} V^2$, and $2u_e v_e \sim 2A^{-1} UV$, for x near x_j. Hence, for x near x_j, the right hand-side of (5.17) is given by

$$\eta v_e^2 + 2u_e v_e \phi \sim \frac{c_j}{\varepsilon} \left(2UVV_y + V^2 U_y \right) = \frac{c_j}{\varepsilon} \left(UV^2 \right)_y . \tag{5.18}$$

Since UV^2 is even, we obtain in the the sense of distributions that

$$\frac{c_j}{\varepsilon} \left(UV^2 \right)_y \to 2\varepsilon B c_j \delta^{'}(x - x_j) , \tag{5.19}$$

where $B \equiv \int_0^\infty UV^2 \, dy$, given in (3.23), is the bifurcation parameter for the core problem (3.11). In this way, the following outer problem for $\eta(x)$ is obtained from (5.17):

$$D\eta_{xx} - (1 + \tau\lambda)\eta = 2\varepsilon B \sum_{i=1}^{k} c_i \delta^{'}(x - x_i) , \quad -1 < x < 1 ; \qquad \eta_x(\pm 1) = 0 . \tag{5.20}$$

The solution to (5.20) can be written as

$$\eta(x) = -2\varepsilon B \sum_{i=1}^{k} c_i g(x; x_i) , \tag{5.21}$$

where $g(x; x_i)$ is the dipole Green's function satisfying

$$D g_{xx} - (1 + \tau\lambda) g = -\delta^{'}(x - x_i) , \qquad -1 < x < 1 ; \qquad g_x(\pm 1; x_i) = 0 . \tag{5.22}$$

To determine $N_{1y}(\infty)$ in (5.16) we use the matching condition that the far-field behavior of the j^{th} inner solution as $y \to +\infty$ must agree with the behavior of (5.21) as $x \to x_j^+$. Defining $y = \varepsilon^{-1}(x - x_j)$, we obtain from (5.4), (5.6), and (5.21), that this matching condition is

$$\frac{\varepsilon}{D}\left(c_j U_y + \frac{\varepsilon A}{\sqrt{D}} N_1\right) \sim \eta(x_j^+) - 2\varepsilon^2 B y \sum_{i=1}^{k} c_i g_x(x_j; x_i) \,. \tag{5.23}$$

The leading terms in (5.23) match identically. To match the remaining terms we require that

$$N_{1y}(\infty) = -\frac{2BD^{3/2}}{A} \sum_{i=1}^{k} c_i g_x(x_j; x_i) = -2\tanh\left(\frac{\theta_0}{k}\right) D^{3/2} \sum_{i=1}^{k} c_i g_x(x_j; x_i) \,. \tag{5.24}$$

Here we have used the relation $A = B\coth(\theta_0/k)$ from (3.12). Substituting (5.24) into (5.16), we obtain the following matrix problem for $\boldsymbol{c} = (c_1, \ldots, c_k)^t$ and λ_0:

$$\lambda_0 \boldsymbol{c} = \alpha \left[2\tanh\left(\frac{\theta_0}{k}\right) D^{3/2} \mathcal{G}_g - I\right] \boldsymbol{c} \,. \tag{5.25}$$

Here α is defined by

$$\alpha \equiv -\frac{\Psi_2^\dagger(\infty)}{\int_0^\infty \Psi_1^\dagger V_y \, dy} \,, \tag{5.26}$$

and $\mathcal{G}_g$ is the dipole Green's matrix defined by

$$\mathcal{G}_g \equiv \begin{pmatrix} g_x(x_1; x_1) & \cdots & g_x(x_1; x_k) \\ \vdots & \ddots & \vdots \\ g_x(x_k; x_1) & \cdots & g_x(x_k; x_k) \end{pmatrix} . \tag{5.27}$$

To solve the matrix problem (5.25), we must determine the eigenvectors and eigenvalues of $\mathcal{G}_g$. Although the matrix $\mathcal{G}_g$ is full, its inverse matrix is tridiagonal (see [18]). More specifically, in Appendix C of [18] it was shown that

$$\mathcal{G}_g = \frac{\sqrt{1+\tau\lambda}}{D^{3/2}} \mathcal{B}_g^{-1} \,, \tag{5.28}$$

where B_g is the tridiagonal matrix

$$\mathcal{B}_g \equiv \begin{pmatrix} d & f & 0 & \cdots & 0 & 0 & 0 \\ f & e & f & \cdots & 0 & 0 & 0 \\ 0 & f & e & \ddots & 0 & 0 & 0 \\ \vdots & \vdots & \ddots & \ddots & \ddots & \vdots & \vdots \\ 0 & 0 & 0 & \ddots & e & f & 0 \\ 0 & 0 & 0 & \cdots & f & e & f \\ 0 & 0 & 0 & \cdots & 0 & f & d \end{pmatrix} , \tag{5.29a}$$

with matrix entries d, e, and f defined by

$$d \equiv \coth\left(\frac{2\theta_\lambda}{k}\right) + \coth\left(\frac{\theta_\lambda}{k}\right), \qquad e \equiv 2\coth\left(\frac{2\theta_\lambda}{k}\right), \qquad f \equiv -\text{csch}\left(\frac{2\theta_\lambda}{k}\right). \tag{5.29b}$$

Here θ_λ is defined by

$$\theta_\lambda \equiv \theta_0\sqrt{1+\tau\lambda}\,, \qquad \theta_0 \equiv D^{-1/2}\,. \tag{5.30}$$

The spectrum of $\mathcal{B}_g$ can be calculated explicitly as was done in Appendix D of [18] (see Proposition 9 of [18]), with the result:

Proposition 5.1: *The eigenvalues ζ_j, ordered as $0 < \zeta_1 < \ldots < \zeta_k$, of $\mathcal{B}_g$ and the associated normalized eigenvectors $\mathbf{c}_j$ of $\mathcal{B}_g$ are*

$$\zeta_j = 2\coth\left(\frac{2\theta_\lambda}{k}\right) - 2\text{csch}\left(\frac{2\theta_\lambda}{k}\right)\cos\left(\frac{\pi j}{k}\right), \qquad j = 1,\ldots,k\,, \tag{5.31a}$$

$$\mathbf{c}_k^t = \frac{1}{\sqrt{k}}\left(1,-1,1,\,\ldots\,,(-1)^{k+1}\right); \quad \mathbf{c}_{l,j} = \sqrt{\frac{2}{k}}\sin\left(\frac{\pi j}{k}(l-1/2)\right), \quad j = 1,\ldots,k-1\,. \tag{5.31b}$$

Here $\mathbf{c}^t$ denotes transpose and $\mathbf{c}_j^t = (c_{1,j},\ldots,c_{k,j})$.

By substituting (5.28) and (5.31) into (5.25), we obtain k transcendental equations for the eigenvalue λ_0. The eigenvectors in (5.31) determine the constants c_j, for $j = 1,..,k$. In this way, we obtain the following main result for the small eigenvalues:

Proposition 5.2: *Let $\varepsilon \ll 1$, and $\varepsilon A/\sqrt{D} \ll 1$. Then, the small eigenvalues λ associated with drift instabilities of the k-spike equilibrium solution of Proposition 3.1 are of order $O\left(\varepsilon A/\sqrt{D}\right)$, and satisfy the k transcendental equations,*

$$\lambda \sim \frac{\varepsilon\alpha A}{\sqrt{D}}\left[\frac{\sqrt{1+\tau\lambda}\tanh(\theta_0/k)\sinh(2\theta_\lambda/k)}{\cosh(2\theta_\lambda/k)-\cos(\pi j/k)} - 1\right], \qquad j = 1,\ldots,k\,, \tag{5.32}$$

where α and θ_λ are defined in (5.26) and (5.30). The constant α depends on the bifurcation parameter γ associated with the core solution. In the inner region near the j^{th} spike, the perturbation to the v-component of the equilibrium solution has the following form for some $\delta \ll 1$:

$$v(x,t) \sim \frac{\sqrt{D}}{\varepsilon}\left(V[\varepsilon^{-1}(x-x_j)] + \delta c_j V_y[\varepsilon^{-1}(x-x_j)]e^{\lambda t}\right). \tag{5.33}$$

For a one-spike solution where $k = 1$, (5.32) can be reduced to

$$\lambda \sim \frac{\varepsilon\alpha A}{\sqrt{D}}\left[\sqrt{1+\tau\lambda}\tanh(\theta_0)\tanh(\theta_\lambda) - 1\right]. \tag{5.34}$$

This expression is very similar in form to the result (2.9b) of Proposition 2.3 in the intermediate parameter regime. The only difference between (5.34) and (2.9b) is in a multiplicative factor. We now show that these two formulae do in fact agree if we let $A \to 0$ in (5.34).

To show this, we must calculate the limiting behavior of α in (5.26) along the primary branch as $B \to 0$ and $\gamma \to 3/2$. In this limit, we recall from Proposition 4.1 that $V \sim \delta w$, and $U \sim \delta^{-1}$, where $\delta \sim A/[3\coth(\theta_0)]$. Here w is the spike profile given in (2.2). Therefore, for $\delta \ll 1$, the homogeneous adjoint problem (5.11) reduces to

$$\psi^\dagger_{1yy} + (-1+2w)\psi^\dagger_1 - 2w\psi^\dagger_2 \sim 0\,, \qquad \psi^\dagger_{2yy} + \delta^2 w^2 \left(\psi^\dagger_1 - \psi^\dagger_2\right) \sim 0\,. \tag{5.35}$$

The solution to this limiting system is odd and is given, up to a normalization constant, by

$$\psi^\dagger_1 = w_y + O(\delta^2)\,, \qquad \psi^\dagger_2 = -\frac{\delta^2}{3}\int_0^y [w(s)]^3\, ds + O(\delta^4)\,. \tag{5.36}$$

Therefore, for $\delta \ll 1$, we have

$$\alpha \equiv -\frac{\Psi^\dagger_2(\infty)}{\int_0^\infty \Psi^\dagger_1 V_y\, dy} \sim \frac{\delta}{3}\left(\frac{\int_0^\infty w^3\, dy}{\int_0^\infty w_y^2\, dy}\right)\,. \tag{5.37}$$

To calculate the integral in (5.37) we use $w(y) = \frac{3}{2}\mathrm{sech}^2(y/2)$. This yields $\alpha = 2\delta$. Then, using $\delta \sim A/[3\coth(\theta_0)]$, and $B = A\tanh\theta_0$, we obtain the limiting result

$$\alpha \sim \frac{2A}{3}\tanh\theta_0 \sim \frac{2B}{3}\,, \qquad \text{for} \quad A \ll 1\,. \tag{5.38}$$

Substituting (5.38) into (5.34) we do indeed recover (2.9b).

To determine α in (5.26) we compute the numerical solution to the adjoint problem (5.11), and then evaluate the integral in (5.26) with a numerical quadrature. In Fig. 6 we plot α versus B along the primary branch in the B, γ parameter plane of Fig. 2(a). Although we are not able to give a rigorous proof of the sign of α, our computations show that $\alpha > 0$ along this branch.

Since $\lambda = O(\varepsilon)$, we have that $\lambda\tau \ll 1$ for $\tau \ll O(\varepsilon^{-1})$. For $\tau \ll O(\varepsilon^{-1})$, it is readily shown that (5.32) reduces to

$$\lambda \sim -\frac{\varepsilon\alpha A}{\sqrt{D}}\left[\frac{1-\cos(\pi j/k)}{\cosh(2\theta_0/k) - \cos(\pi j/k)}\right]\,, \qquad j = 1,\ldots,k\,, \tag{5.39}$$

Since $\alpha > 0$, we conclude that $\lambda < 0$ for $j = 1,\ldots,k$. This leads to the following stability result:

Proposition 5.3: *Let $\varepsilon \ll 1$, $\tau \ll O(\varepsilon^{-1})$, and $\varepsilon A/\sqrt{D} \ll 1$. Then, along the primary branch of the B, γ parameter plane, the k-spike equilibrium solution of Proposition 3.1 is stable with respect to drift instabilities associated with the small eigenvalues.*

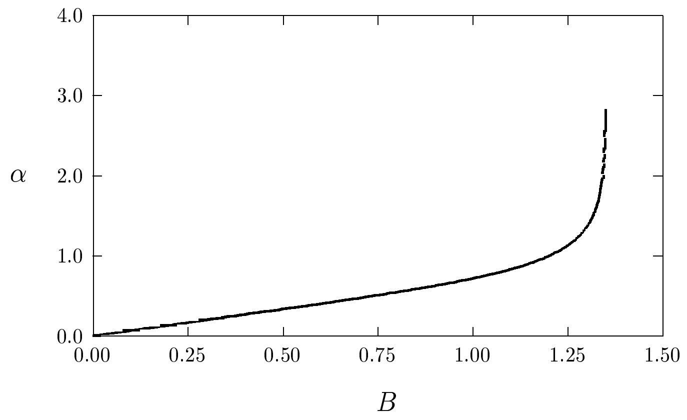

Figure 6: Plot of α, defined in (5.26), versus B along the primary solution branch of the B, γ parameter plane. The right endpoint of this curve corresponds to the fold point $B = 1.347$.

We now determine instabilities associated with (5.32) when $\lambda = O(\varepsilon^{-1})$. To analyze (5.32) it is convenient to introduce the new variables τ_d, ω, and ξ, defined by

$$\lambda = \left(\frac{\varepsilon\alpha A}{\sqrt{D}}\right)\omega\,, \qquad \tau = \left(\frac{\sqrt{D}}{\varepsilon\alpha A}\right)\tau_d\,, \qquad \xi = \tau_d\omega\,. \tag{5.40}$$

Substituting (5.40) into (5.32), we obtain that ξ satisfies $F_j(\xi) = 0$, where

$$F_j(\xi) \equiv \frac{\xi}{\tau_d} - G_j(\xi)\,, \qquad G_j(\xi) \equiv \frac{\sqrt{1+\xi}\tanh\left(\theta_0/k\right)\sinh\left(2\theta_0\sqrt{1+\xi}/k\right)}{\cosh\left(2\theta_0\sqrt{1+\xi}/k\right) - \cos\left(\pi j/k\right)} - 1\,, \qquad j = 1,\ldots,k\,. \tag{5.41}$$

In terms of the roots $F(\xi) = 0$, the scaled eigenvalues ω are given by $\omega = \xi/\tau_d$.

For the one-spike case $k = 1$, (5.41) reduces to the problem (2.11) considered in §2 for the small eigenvalue of a one-spike solution in the intermediate regime. Therefore, Proposition 2.4 of §2 proved in [19] also applies to the stability of a one-spike solution in the pulse-splitting regime.

Proposition 5.4: *Let $\varepsilon \ll 1$, $\tau = O(\varepsilon^{-1})$, $k = 1$, and $\varepsilon A/\sqrt{D} \ll 1$. Then, there exists a unique value τ_{dh}, depending on D, for which there is a complex conjugate pair of pure imaginary eigenvalues when $\tau_d = \tau_{dh}$. For any $\tau_d > \tau_{dh}$ there are exactly two eigenvalues in the right half-plane. These eigenvalues merge onto the positive real axis when $\tau_d = \tau_{dm}$, and they remain there for all $\tau_d > \tau_{dm}$. In terms of*

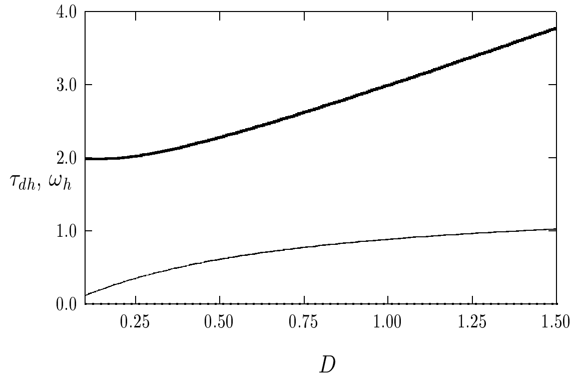

(a) τ_{dh} and ω_h

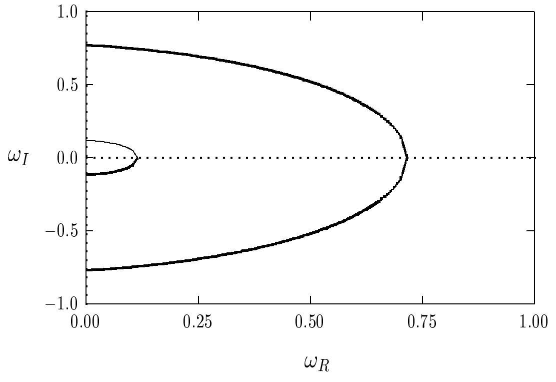

(b) eigenvalues in right half-plane

Figure 7: A one-spike solution. Left figure: The Hopf bifurcation value τ_{dh} (heavy solid curve) and the frequency ω_h (solid curve) versus D. Right figure: The eigenvalues $\omega = \omega_R + i\omega_I$ in the right half-plane for $\tau_{dh} \leq \tau \leq \tau_{dm}$ when $D = 0.75$ (heavy solid curve) and $D = 0.1$ (solid curve).

τ, the Hopf bifurcation in the spike location occurs when $\tau = \tau_{TW}$, where

$$\tau_{TW} \sim \left(\frac{\sqrt{D}}{\varepsilon \alpha A} \right) \tau_d \, . \tag{5.42}$$

To determine τ_{dh} for a one-spike solution where $k = 1$ we numerically determine the zeroes of $F_1(\xi) = 0$ on the imaginary axis. The zeroes occur when $\xi = i\xi_h$ and $\tau_d = \tau_{dh}$, which yields $\omega_h \equiv \xi_h/\tau_{dh}$. In Fig. 7(a) we plot τ_{dh} and ω_h versus D. To illustrate Proposition 5.4, we compute the roots of $F_1(\xi) = 0$ with $\xi = \xi_R + i\xi_I$ on the range $\tau_{dh} \leq \tau_d \leq \tau_{dm}$. In terms of $\omega = \xi/\tau_d \equiv \omega_R + i\omega_I$, in Fig. 7(b) we plot this path in the complex plane for $D = 0.75$ and $D = 0.1$.

We now consider the multi-spike case where $k > 1$. We first look for roots of $F_j(\xi) = 0$ on the positive imaginary axis $\xi = i\xi_I$ with $\xi_I \geq 0$. By separating (5.41) into real and imaginary parts, we obtain

$$F_{jR}(\xi_I) = -G_{jR}(\xi_I) \, , \qquad F_{jI}(\xi_I) = \frac{\xi_I}{\tau_d} - G_{jI}(\xi_I) \, , \qquad j = 1, \ldots, k \, , \tag{5.43}$$

where $F_{jR}(\xi_I) = \text{Re}(F_j(i\xi_I))$, $F_{jI}(\xi_I) = \text{Im}(F_j(i\xi_I))$, $G_{jR}(\xi_I) = \text{Re}(G_j(i\xi_I))$, and $G_{jI}(\xi_I) = \text{Re}(G_j(i\xi_I))$.

Using (5.41), it is readily seen that $G_{jR}(0) < 0$ and that $G_{jR}(\xi_I)$ is monotonically increasing with $G_{jR}(\xi_I) \to +\infty$ as $\xi_I \to \infty$. Therefore, $F_{jR}(\xi_I) = 0$ has a unique root, which we label by ξ_{Ij}. Then, setting $F_{jI}(\xi_{Ij}) = 0$, we obtain the critical value τ_{dj}, defined by

$$\tau_{dj} \equiv \frac{\xi_{Ij}}{G_{jI}(\xi_{Ij})}, \qquad j = 1, \ldots, k. \tag{5.44}$$

In terms of τ_{dj}, we define $\omega_j \equiv \xi_{Ij}/\tau_{dj}$. For each j, τ_{dj} denotes the unique value of τ_d where there is a complex conjugate pair of small eigenvalues on the imaginary axis.

By adapting the proof of Proposition 5.6 of [19], we can prove that, for each fixed $j = 1, \ldots, k$, there are exactly two roots of $F_j(\xi) = 0$ for any $\tau_d > \tau_{dj}$. In addition, these roots merge onto the positive real axis when $\tau_d = \tau^*_{dj} > \tau_{dj}$, and they remain there for $\tau_d > \tau^*_{dj}$. To show this, we first derive a formula for the number M_j of zeroes of $F_j(\xi) = 0$ in the right half-plane. To do so, we calculate the winding number of $F_j(\xi)$ over the counterclockwise contour composed of the imaginary axis $-iR \leq \mathrm{Im}(\xi) \leq iR$ and the semi-circle Γ_R, given by $|\xi| = R > 0$, for $\mathrm{Re}(\xi) > 0$. For any $\tau_d > 0$, it is easy to see from (5.41) that the change in the argument of $F_j(\xi)$ over Γ_R as $R \to \infty$ is π. Since $F_j(\xi)$ is analytic in $\mathrm{Re}(\xi) \geq 0$, and $F_j(\overline{\xi}) = \overline{F_j(\xi)}$, the argument principle yields that

$$M_j = \frac{1}{2} + \frac{1}{\pi} \left[\arg F_j\right]_{\Gamma_I}. \tag{5.45}$$

Here $\left[\arg F_j\right]_{\Gamma_I}$ denotes the change in the argument of $F_j(\xi)$ along the semi-infinite imaginary axis $\Gamma_I = i\xi_I$, $0 \leq \xi_I < \infty$, traversed in the downwards direction.

To calculate M_j, we note that $F_{jI} = O(\xi_I)$ and $F_{jR} = O(\sqrt{\xi_I})$ as $\xi_I \to \infty$, and that $F_{jI}(0) = 0$ with $F_{jR}(0) > 0$. This implies that $\arg F_j = \pi/2$ as $\xi_I \to +\infty$, and $\arg F_j = 0$ at $\xi_I = 0$. Since the root to $F_{jR}(\xi_I) = 0$ is unique and independent of τ_d, the change in the argument $\left[\arg F_j\right]_{\Gamma_I}$ is determined by the sign of $F_{jI}(\xi_I)$ at the unique root of $F_{jR}(\xi_I) = 0$. In this way, we get that $\left[\arg F_j\right]_{\Gamma_I}$ is $3\pi/2$ when $\tau > \tau_{dj}$ and is $-\pi/2$ when $0 < \tau_d < \tau_{dj}$. From (5.45) this yields that $M_j = 2$ when $\tau_d > \tau_{dj}$ and $M_j = 0$ when $0 < \tau_d < \tau_{dj}$. Therefore, the roots of $F_j(\xi) = 0$ have a strict transversal crossing into the right half-plane as τ is increased past τ_{dj}. The fact that that the roots of $F_j(\xi) = 0$ merge onto the real axis at some value τ^*_{dj} follows from the simple observation that $G_j(\xi)$ in (5.41) is an increasing, and concave, function when $\xi > 0$ is real, and that $G_j(0) < 0$. This proves that when ξ is real, $F_j(\xi) = 0$ will have exactly two roots for $\tau \geq \tau^*_{dj}$, where τ^*_{dj} is determined from the condition that ξ/τ_d intersects $G_j(\xi)$ tangentially at a unique point when $\tau = \tau^*_{dj}$. This leads to the following stability result for a k-spike solution:

Proposition 5.5: *Let $\varepsilon \ll 1$, $\tau = O(\varepsilon^{-1})$, and $\varepsilon A/\sqrt{D} \ll 1$. Then, along the primary branch of the B, γ parameter plane, the k-spike equilibrium solution of Proposition 3.1 is stable when $0 < \tau < \tau_{TW}$, and is unstable when $\tau > \tau_{TW}$. The stability of this solution is lost due to a Hopf bifurcation in the*

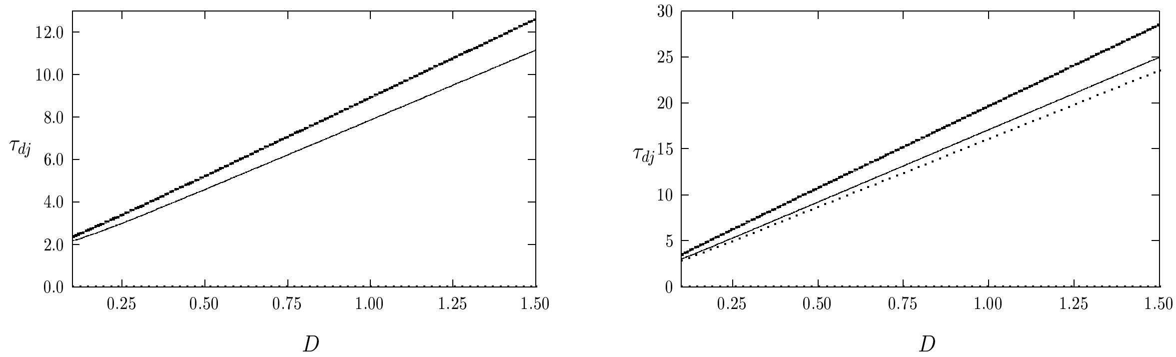

(a) Two spikes: τ_{dj} for $j = 1, 2$

(b) Three spikes: τ_{dj} for $j = 1, 2, 3$

Figure 8: The values τ_{dj} for $j = 1, \ldots, k$ versus D where complex conjugate eigenvalues enter the right half-plane. The Hopf bifurcation value τ_{dh} is the minimum of these values. Left figure: a two-spike solution, with $j = 1$ (heavy solid curve) and $j = 2$ (solid curve). Right figure: a three-spike solution with $j = 1$ (heavy solid curve), $j = 2$ (solid curve), and $j = 3$ (dashed curve).

spike locations that occurs when $\tau = \tau_{TW}$, where

$$\tau_{TW} \sim \left(\frac{\sqrt{D}}{\varepsilon \alpha A} \right) \tau_{dh} \,, \qquad \tau_{dh} \equiv \min_{j=1,\ldots,k} (\tau_{dj}) \,. \tag{5.46}$$

For a two-spike solution where $k = 2$, in Fig. 8(a) we plot the numerically computed functions τ_{dj} for $j = 1, 2$ versus D. A similar plot for the three-spike case is shown in Fig. 8(b). These numerical results, together with other results (not shown) for larger ranges of D and for $k > 3$, suggest that in each case τ_{dh} is determined by the $j = k$ mode. From (5.31b), we see that the effect of the $j = k$ mode on the small-scale oscillatory behavior of the spike locations is to introduce a breathing-type instability whereby consecutive spike-layer locations are 180° degrees out of phase. This leads to the following conjecture:

Conjecture 5.6: *Let $\varepsilon \ll 1$, and $\varepsilon A/\sqrt{D} \ll 1$. Then, along the primary branch, a k-spike solution first loses its stability to a breathing-type instability at the value $\tau = \tau_{TW} \sim \left(\frac{\sqrt{D}}{\varepsilon \alpha A} \right) \tau_{dk}$. In terms of the v-component, this small-scale oscillatory instability takes the form,*

$$v(x,t) \sim \frac{\sqrt{D}}{\varepsilon} \sum_{j=1}^{k} V\left(\varepsilon^{-1}[x - x_j(t)] \right) \,, \qquad x_j(t) \sim x_j(0) + \delta c_j \cos\left(\frac{\varepsilon \alpha A \omega_k t}{\sqrt{D}} - \phi \right) \,, \tag{5.47}$$

where $\delta \ll 1$, and ϕ is arbitrary. Here $c_j = (-1)^j$ and $x_j(0) = -1 + (2j-1)/k$ for $j = 1, \ldots, k$. In addition, $\omega_k = \xi_{Ik}/\tau_{dk}$, where $F_k(i\xi_{Ik}) = 0$.

6 Stability of the Profile: The Large Eigenvalues

We now determine the stability of the k-spike equilibrium solution of Proposition 3.1 with respect to eigenvalues λ with $\lambda = O(1)$ as $\varepsilon \to 0$. Assuming that $\tau \ll O(\varepsilon^{-2})$, we can repeat the calculation from (5.1)-(5.5) to derive the following leading order eigenvalue problem in the j^{th} inner region:

$$\Phi_{0yy} - \Phi_0 + 2UV\Phi_0 + V^2 N_0 = \lambda\Phi_0\,, \quad -\infty < y < \infty\,, \tag{6.1a}$$

$$N_{0yy} - V^2 N_0 - 2UV\Phi_0 = 0\,, \quad -\infty < y < \infty\,. \tag{6.1b}$$

We seek an even eigenfunction of (6.1) for which $\Phi_0 \to 0$. Upon matching to the outer region below, the other boundary condition is that $N_{0y} \to 0$ as $|y| \to \infty$.

To derive such an asymptotic boundary condition for N_0, we consider the outer solution for η given in (5.17). Since Φ_0 and N_0 are even, we obtain in place of (5.18) that near x_j,

$$\eta v_e^2 + 2u_e v_e \phi \sim \frac{1}{\varepsilon}\left(2UV\Phi_0 + V^2 N_0\right) \sim \frac{1}{\varepsilon} N_{0yy}\,. \tag{6.2}$$

Therefore, since N_{0y} is odd, we get in place of (5.20) that

$$D\eta_{xx} - (1+\tau\lambda)\eta = 2\sum_{i=1}^{k} N_{0y}(\infty)\delta(x - x_i)\,, \quad -1 < x < 1\,; \qquad \eta_x(\pm 1) = 0\,. \tag{6.3}$$

The solution to (6.3) can be written as

$$\eta(x) = -2\sum_{i=1}^{k} N_{0y}(\infty) G(x; x_i)\,, \tag{6.4}$$

where $G(x; x_i)$ is the Green's function satisfying (2.3). The leading order matching condition analogous to (5.23) is that $\varepsilon D^{-1} N_0$ as $|y| \to \infty$ agrees with $\eta(x)$ as $x \to x_j$. This enforces that $N_{0y}(\infty) = 0$. Therefore, the leading order eigenvalue problem (6.1) is universal in that it does not involve a coupling of the eigenvalue problems associated with each inner region.

We now consider the spectrum of (6.1). Recall from the core problem (3.11) that at the fold point $\gamma = \gamma_c$ of the $B = B(\gamma)$ curve, we have that $B'(\gamma_c) = 0$. This implies that (6.1) has an eigenfunction

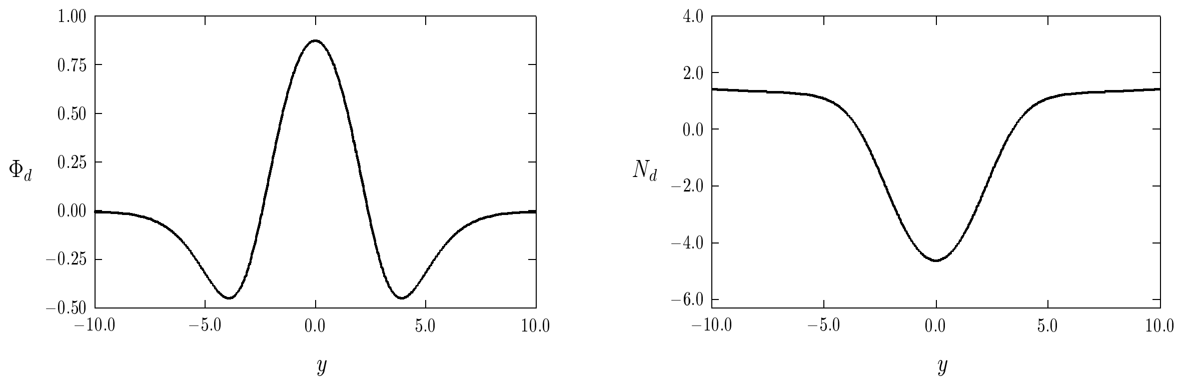

(a) $\Phi_d(y)$ (b) $N_d(y)$

Figure 9: The dimple eigenfunction $\Phi_d = V_\gamma(y)$ (left figure) and $N_d = U_\gamma(y)$ (right figure) at $\gamma = \gamma_c \approx 1.02$.

with zero eigenvalue at this point. To see this, we differentiate the leading order core problem (3.11) and (3.13) with respect to γ to get

$$V_\gamma'' - V_\gamma + 2UVV_\gamma + V^2U_\gamma = 0\,, \qquad -\infty < y < \infty\,, \tag{6.5a}$$

$$U_\gamma'' = U_\gamma V^2 + 2UVV_\gamma\,, \qquad -\infty < y < \infty\,, \tag{6.5b}$$

$$V_\gamma \to 0\,, \qquad U_\gamma \sim B'(\gamma)|y| + \chi'(\gamma)\,, \qquad \text{as} \quad y \to \pm\infty\,. \tag{6.5c}$$

Therefore, at the fold point where $\gamma = \gamma_c$ and $B'(\gamma_c) = 0$, we compare (6.1) and (6.5) to conclude that

$$\Phi_0(y) = \Phi_d(y) \equiv V_\gamma\,, \qquad N_0(y) = N_d(y) \equiv U_\gamma\,, \quad \text{when} \quad \gamma = \gamma_c\,, \tag{6.6}$$

is an eigenfunction of (6.1) with $\lambda = 0$. This eigenfunction Φ_d, which is computed numerically, is shown is shown in Fig. 9 to have a dimple shape. This dimple property was also observed in [28].

We now determine the spectrum of (6.1) numerically as a function of γ. We discretize (6.1) on the interval $[0, L]$ using centered differences, ensuring that Φ and N are even functions and that $N_y \to 0$ at $y = L$. We label $y_1 = 0$, $y_m = L$, with $m > 1$, and we choose a meshsize $h = L/(m-1)$. This leads to the discrete formulation

$$(\mathcal{M} - I + \Lambda_2)\,\mathbf{\Phi_0} + \Lambda_1 \boldsymbol{N_0} = \lambda \mathbf{\Phi_0}\,, \qquad (\mathcal{M} - \Lambda_1)\,\boldsymbol{N_0} = \Lambda_2 \mathbf{\Phi_0}\,, \tag{6.7a}$$

so that

$$\left(\mathcal{M} - I + \Lambda_2 + \Lambda_1 \left(\mathcal{M} - \Lambda_1\right)^{-1} \Lambda_2\right) \mathbf{\Phi_0} = \lambda \mathbf{\Phi_0} \,. \tag{6.7b}$$

Here $\mathbf{\Phi_0} = (\Phi_0(y_1), \ldots, \Phi_0(y_m))^t$, $\boldsymbol{N_0} = (N_0(y_1), \ldots, N_0(y_m))^t$, and the matrices Γ_1, Γ_2, and $\mathcal{M}$, are defined by

$$\Lambda_1 \equiv \begin{pmatrix} V^2(y_1) & 0 & \cdots & 0 \\ 0 & \ddots & \cdots & 0 \\ \vdots & \vdots & \ddots & \vdots \\ 0 & 0 & \cdots & V^2(y_m) \end{pmatrix}, \qquad \Lambda_2 \equiv \begin{pmatrix} 2U(y_1)V(y_1) & 0 & \cdots & 0 \\ 0 & \ddots & \cdots & 0 \\ \vdots & \vdots & \ddots & \vdots \\ 0 & 0 & \cdots & 2U(y_m)V(y_m) \end{pmatrix}, \tag{6.7c}$$

and

$$\mathcal{M} \equiv \frac{1}{h^2} \begin{pmatrix} -2 & 2 & 0 & \cdots & 0 & 0 & 0 \\ 1 & -2 & 1 & \ddots & \ddots & 0 & 0 \\ 0 & \ddots & \ddots & \ddots & \ddots & \ddots & 0 \\ \vdots & \ddots & \ddots & \ddots & \ddots & \ddots & \vdots \\ 0 & \ddots & \ddots & \ddots & \ddots & \ddots & 0 \\ 0 & 0 & \ddots & \ddots & 1 & -2 & 1 \\ 0 & 0 & 0 & \cdots & 0 & 2 & -2 \end{pmatrix} . \tag{6.7d}$$

The eigenvalues of the discrete problem (6.7b) were computed using LAPACK [1] on a domain with $L = 12$ and $m = 200$. Increasing the number of meshpoints and the domain length did not change the results noticeably. In Fig. 10(a) and Fig. 10(b) we plot the real and imaginary parts of the eigenvalues as a function of γ. The plot in Fig. 10(a) shows that the primary solution branch of Fig. 2(a) corresponding to $1.02 < \gamma < 1.5$ is stable with respect to the large eigenvalues, while the secondary branch corresponding to $0 < \gamma < 1.02$ is unstable due to positive real eigenvalue.

For D small, we have shown in Proposition 3.2 that there is an approximate lining-up property of k-spike equilibrium branches associated with the core solution. Moreover, the numerical computations above have shown that there is a dimple-shaped eigenfunction at the saddle-node bifurcation point A_{pk}. In addition, we have shown numerically that the primary solution branch is stable with respect to the large eigenvalues when $\tau \ll O(\varepsilon^{-2})$, but that the secondary branch is always unstable. In §5 we showed that the primary solution branch is stable with respect to drift instabilities when $\tau \ll O(\varepsilon^{-1})$. Therefore, the pulse-splitting criteria of [10] are satisfied when $\tau \ll O(\varepsilon^{-1})$. This leads us to the following conjecture concerning the number of pulse-splitting events and the final equilibrium state for a dynamical process under (1.3):

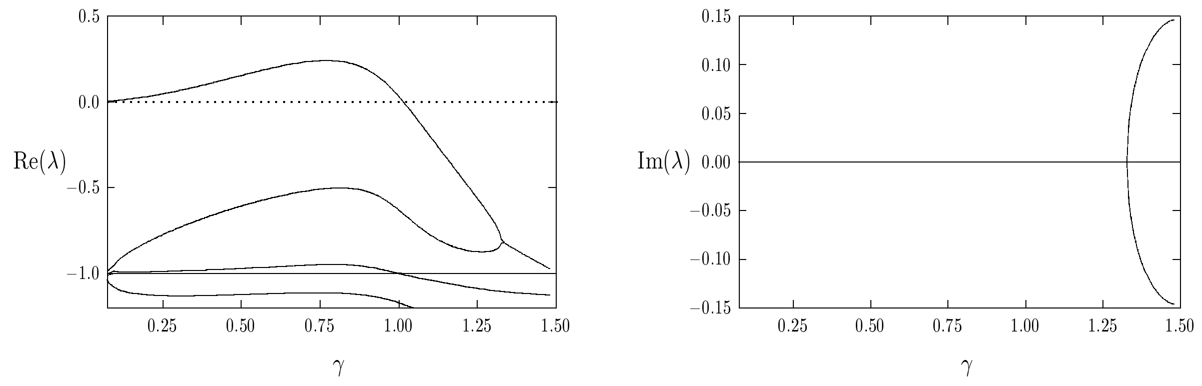

(a) Re(λ) versus γ (b) Im(λ) versus γ

Figure 10: Left figure: Re(λ) versus γ for the spectrum of (6.1). There is an eigenvalue with a positive real part only when $0 < \gamma < 1.02$. Right figure: Im(λ) versus γ for the spectrum of (6.1).

Conjecture 6.1: *Let $\varepsilon \ll 1$, $\tau \ll O(\varepsilon^{-1})$, and $\varepsilon A/\sqrt{D} \ll 1$. Suppose that we have even one-spike initial data centered at the origin. Then, the final equilibrium state is stable with respect to both the large and small eigenvalues, and it has 2^m spikes where, for some integer $m \geq 0$, A satisfies*

$$A_{p2^{m-1}} < A < A_{p2^m} \,. \tag{6.8}$$

Here A_{pk} is the existence threshold, which depends on D, defined in (3.28).

Finally, we determine whether the primary solution branch can become unstable with respect to a Hopf bifurcation of the large eigenvalues when $\tau = O(\varepsilon^{-2})$. For this range of τ, the slow drift instabilities of §5 are also present. In (5.5) we let $\tau = O(\varepsilon^{-2})$. In place of (6.1), we then obtain the following eigenvalue problem on $-\infty < y < \infty$:

$$\Phi_{0yy} - \Phi_0 + 2UV\Phi_0 + V^2 N_0 = \lambda \Phi_0 \,; \qquad N_{0yy} - V^2 N_0 - 2UV\Phi_0 = \lambda \tau_L N_0 \,, \tag{6.9a}$$

where

$$\tau = \frac{D\tau_L}{\varepsilon^2} \,. \tag{6.9b}$$

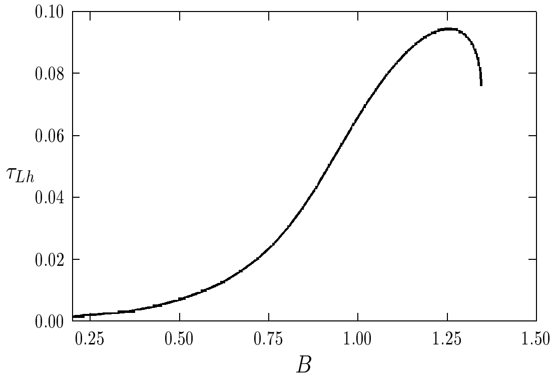

(a) τ_{Lh} versus B

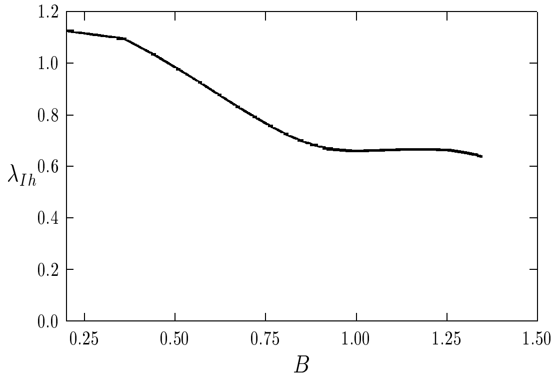

(b) λ_{Ih} versus B

Figure 11: Left figure: There is a Hopf bifurcation in the spike amplitude when $\tau = D\tau_{Lh}/\varepsilon^2$. Right figure: the value $\lambda = i\lambda_{Ih}$ where there is a pair of complex conjugate eigenvalues on the imaginary axis.

In place of (6.7), the eigenvalues of (6.9) are approximated by the discrete eigenvalues of the block matrix problem

$$\begin{pmatrix} \mathcal{M} - I + \Lambda_2 & \Lambda_1 \\ -\Lambda_2 & \mathcal{M} - \Lambda_1 \end{pmatrix} \begin{pmatrix} \mathbf{\Phi_0} \\ \boldsymbol{N_0} \end{pmatrix} = \begin{pmatrix} I & 0 \\ 0 & \tau_L I \end{pmatrix} \begin{pmatrix} \mathbf{\Phi_0} \\ \boldsymbol{N_0} \end{pmatrix} . \tag{6.10}$$

For each τ_L, we compute the discrete eigenvalues using a generalized eigenvalue problem solver from LAPACK [1]. Newton's method is then used to determine the value τ_{Lh} of τ_L where eigenvalues first enter the right half-plane. The computations show that these eigenvalues enter the right half-plane through a Hopf bifurcation. In Fig. 11(a) and Fig. 11(b) we plot the Hopf bifurcation value τ_{Lh} and the corresponding $\text{Im}(\lambda) = \lambda_{Ih}$ for each point along the primary solution branch.

7 Numerical Experiments

In this section we perform some numerical experiments on (1.3) to test Conjectures 5.6 and 6.1, and to illustrate instabilities that can occur when τ is asymptotically large. The numerical results below are computed using the routine D03PCF of the NAG library [29] with 1500 uniformly spaced meshpoints.

The initial condition for (1.3) is taken to be

$$v(x,0) = \frac{\sqrt{D}}{\varepsilon} V(0) \sum_{j=1}^{k} \text{sech}^2 \left(\frac{\varepsilon^{-1}(x - x_j)}{2} \right) , \qquad u(x) = 1 - \left(1 - \frac{\varepsilon}{A\sqrt{D}} U(0) \right) \sum_{j=1}^{k} G(x; x_j)/a_g \, . \tag{7.1}$$

Here a_g is defined in (2.1d). In addition, $U(0)$, $V(0)$ denote the solution to the core problem (3.11) at $y = 0$ and at the fold point where $\gamma = \gamma_c$.

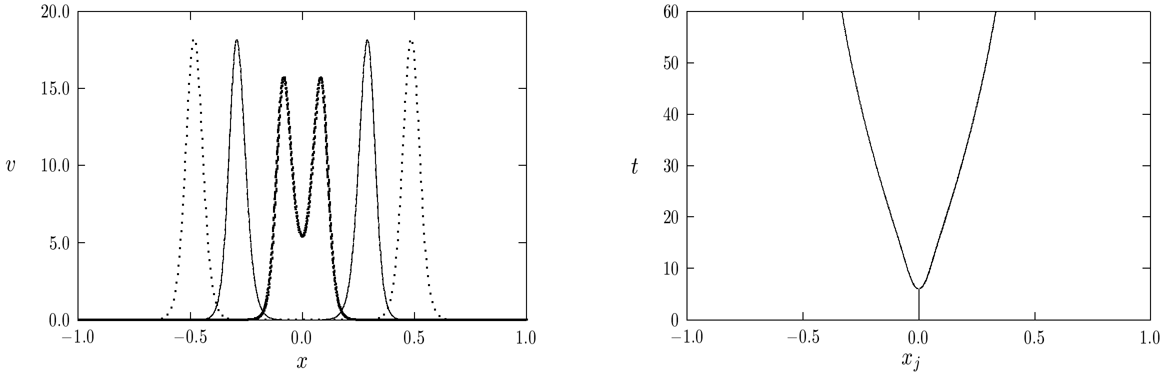

(a) v versus x

(b) t versus x_j

Figure 12: Experiment 1: the parameters are $\varepsilon = 0.02$, $k = 1$, $D = 0.75$, $A = 2.0$, and $\tau = 2.0$. Left figure: the solution v at $t = 8.05$ (heavy solid curve), $t = 15$ (solid curve), and $t = 50.2$ (dashed curve). Right figure: t versus x_j showing a pulse-splitting event at $t \approx 6.0$.

Experiment 1-2: We consider a one-spike initial condition for (1.3) with $\varepsilon = 0.02$, $D = 0.75$, $A = 2.0$, and $\tau = 2.0$. For these parameter values we get $\varepsilon A/\sqrt{D} = 0.046 \ll 1$, and we compute from (3.28) that $A_{p1} = 1.644$, $A_{p2} = 2.587$, and $A_{p4} = 4.795$. Since $A_{p1} < A < A_{p2}$, there is no one-spike equilibrium solution and we predict only one pulse-splitting event. The final state should be a two-spike solution. In Fig. 12(a) we plot the numerically computed solution v at three different times. In Fig. 12(b) we plot the locations x_j of the maxima of v as a function of time. Indeed, the pulse does only split once, and at the value $t \approx 6.0$. Next, we keep the same parameter values, but increase A to $A = 3.0$, so that $\varepsilon A/\sqrt{D} = 0.069 \ll 1$. In this case, since $A_{p2} < A < A_{p4}$, we now expect that there will be two pulse-splitting events and that the final state will be a four-spike solution. In Fig. 13(a) we plot the numerically computed solution v at three different times, and in the t versus x_j plot of Fig. 13(b) we show that there are two pulse-splitting events, which occur at $t \approx 2.0$ and $t \approx 60.0$.

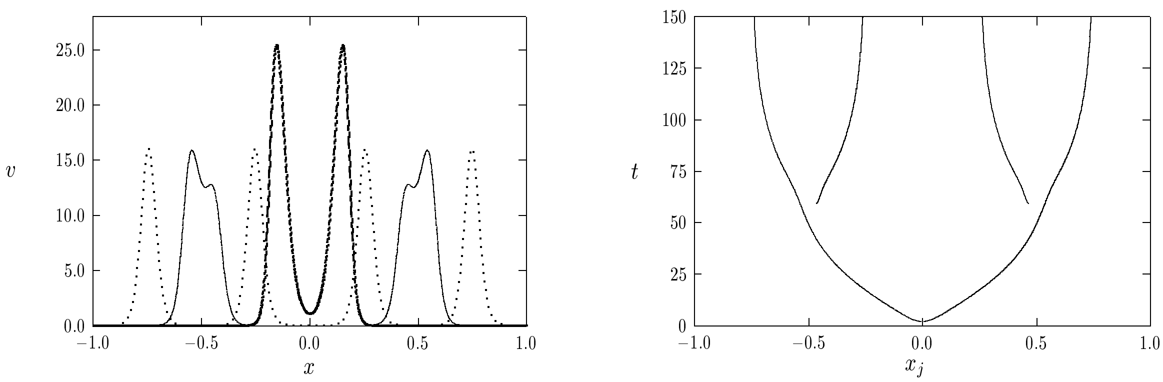

(a) v versus x

(b) t versus x_j

Figure 13: Experiment 2: the parameters are $\varepsilon = 0.02$, $k = 1$, $D = 0.75$, $A = 3.0$, and $\tau = 2.0$. Left figure: the solution v at $t = 10.0$ (heavy solid curve), $t = 61$ (solid curve), and $t = 100$ (dashed curve). Right figure: t versus x_j showing pulse-splitting events at $t \approx 2.0$ and $t \approx 60.0$.

Experiment 3: We now consider a one-spike initial condition for (1.3) with $\varepsilon = 0.01$, $D = 0.1$, $A = 2.4$, and $\tau = 2.0$. This is the example in the introduction §1. For these parameter values we get $\varepsilon A/\sqrt{D} = 0.076$, and from (3.28) we calculate that $A_{p1} = 1.352$, $A_{p2} = 1.466$, $A_{p4} = 2.045$, and $A_{p8} = 3.583$. Since, $A_{p4} < A < A_{p8}$, we expect that there will be three pulse-splitting events, and that the final equilibrium state will be an eight-spike solution. This is indeed what is observed in Fig. 1(b) where we plotted t versus the locations x_j of the maxima of v. There are three pulse-splitting events at $t \approx 2.0$, $t \approx 40.0$, and $t \approx 138$. The gaps in the plot of t versus x_j near the splitting times occur since it is difficult to determine well-defined maxima of v during the pulse-splitting events. The solution is plotted at different times in Fig. 14(a) and Fig. 14(b).

Experiment 4: Next, we consider a three-spike initial condition for (1.3) with $\varepsilon = 0.01$, $D = 0.1$, $A = 1.9$, and $\tau = 2.0$. For these parameter values we get $\varepsilon A/\sqrt{D} = 0.06$, and we compute from (3.28) that $A_{p3} = 1.719$, and $A_{p6} = 2.788$. Since, $A_{p3} < A < A_{p6}$, we predict that there will be one pulse-splitting event, and that the final equilibrium state will be a six-spike solution. This is indeed what is observed in Fig. 15(a) and Fig. 15(b), where we plot the solution v at different times and the

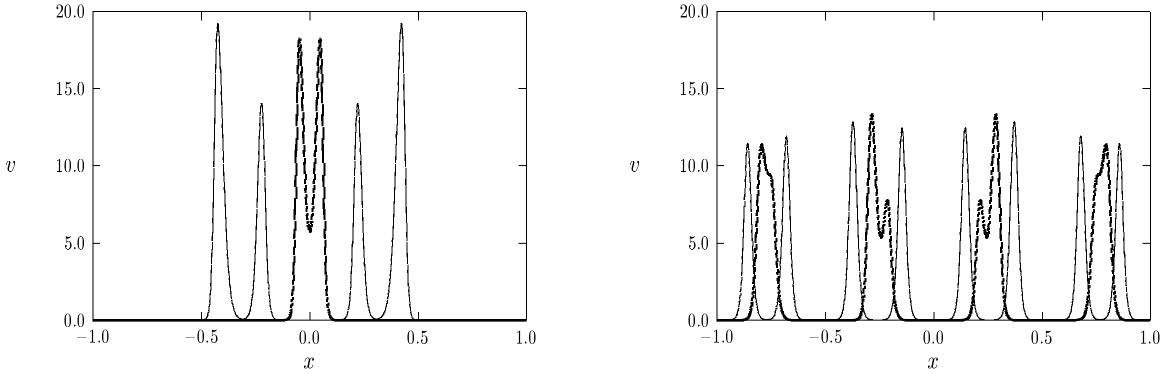

(a) v versus x

(b) v versus x

Figure 14: Experiment 3: the parameters are $\varepsilon = 0.01$, $k = 1$, $D = 0.1$, $A = 2.4$, and $\tau = 2.0$. Left figure: the solution v at $t = 6.0$ (heavy solid curve), $t = 55$ (solid curve). Right figure: v at $t = 145$ (heavy solid curve) and $t = 190$ (solid curve). Pulse-splitting events are at $t \approx 2..0, 40.0, 138.0$.

spike locations t versus x_j, respectively. The pulse-splitting event occurs at $t = 19.5$.

Experiment 5: Next, we consider data for a one-spike initial condition used in Fig. 4 of [6] and Fig. 2b of [5] (see the discussion in §8). The data in Fig. 4 of [6] corresponds to $\varepsilon = 0.00918$, $D = 0.04$, $A = 2.109$, and $\tau = 4.74$. Although D is smaller than in the previous experiments, we still calculate that $\varepsilon A/\sqrt{D} = 0.097 \ll 1$. Therefore, the correction terms to the core solution are still relatively small. For these parameter values, we calculate from (3.28) that $A_{p1} = 1.347$, $A_{p2} = 1.365$, $A_{p4} = 1.588$, and $A_{p8} = 2.429$. Since $A_{p4} < A < A_{p8}$, we predict that there will be three pulse-splitting events, and that the final equilibrium state will be an eight-spike solution. This is indeed what is observed in [6]. In Fig. 16(a) we plot t versus the spike locations x_j, showing splitting events at $t \approx 2.0$, $t \approx 48$, and $t \approx 140$. Next, the data of Fig. 2b of [5] corresponds to $\varepsilon = 0.0077$, $D = 0.04$, $A = 1.483$, and $\tau = 6.74$, so that $\varepsilon A/\sqrt{D} = 0.057$. Since $A_{p2} < A < A_{p4}$, and $\tau \ll O(\varepsilon^{-1})$, we predict that the final equilibrium state will have four spikes. This is what is observed in Fig. 16(b) (see Fig. 2b of [5]).

Experiment 6: Next, we consider one-spike initial data that is not centered at the origin. In the two experiments below we chose $\varepsilon = 0.02$, $D = 0.75$, $\tau = 2.0$, and we take the initial spike to be centered at $x_0(0) = 0.35$. For these parameter values, we calculate from (3.28) that $A_{p1} = 1.644$, $A_{p2} = 2.587$, $A_{p3} = 3.6707$, and $A_{p4} = 4.7950$. For $A = 3.0$, in Fig. 17(a) we plot t versus the spike locations

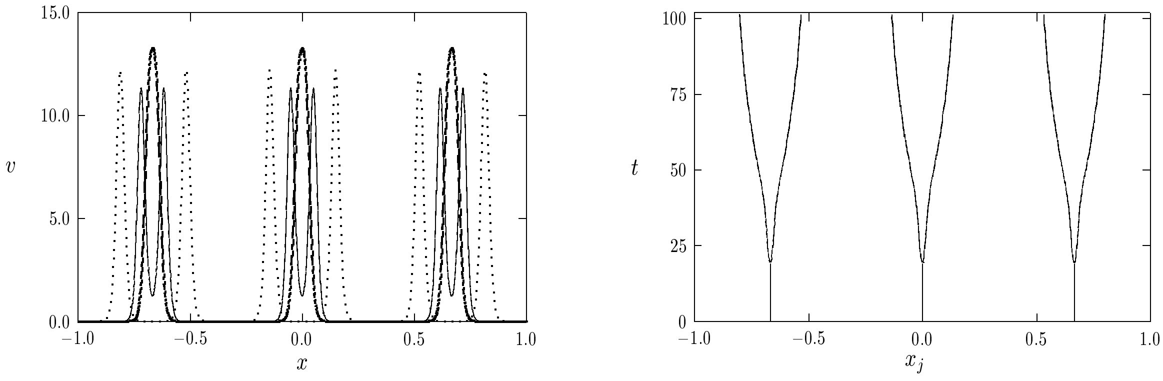

(a) v versus x

(b) t versus x_j

Figure 15: Experiment 4: the parameters are $\varepsilon = 0.01$, $k = 3$, $D = 0.1$, $A = 1.9$, and $\tau = 2.0$. Left figure: the solution v at $t = 10.0$ (heavy solid curve), $t = 50$ (solid curve), and $t = 100$ (dashed curve). Right figure: t versus x_j showing a pulse-splitting event at $t \approx 20.0$.

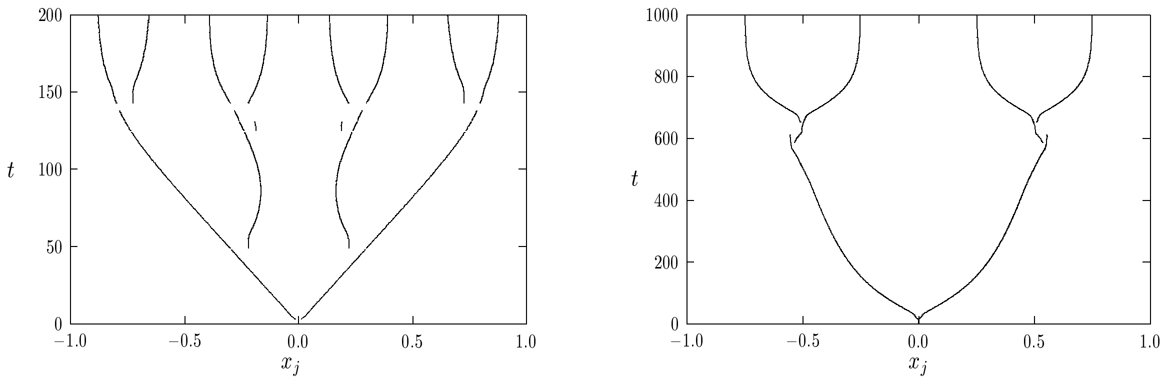

(a) t versus x_j

(b) t versus x_j

Figure 16: Experiment 5: Left figure: t versus x_j for the parameter set $\varepsilon = 0.00918$, $k = 1$, $D = 0.04$, $A = 2.109$, and $\tau = 4.74$. Right figure: t versus x_j when $\varepsilon = 0.0077$, $k = 1$, $D = 0.04$, $A = 1.483$, and $\tau = 6.74$.

x_j, showing one splitting event and a three-spike final equilibrium state. Alternatively, for the value $A = 4.0$, in Fig. 17(b) we show a four-spike final equilibrium state. For the first value of A, where $A_{p2} < A < A_{p3}$, our theory predicts either a three or a four-spike final equilibrium state. A detailed analysis of the dynamics of these patterns is needed to determine the final equilibrium state.

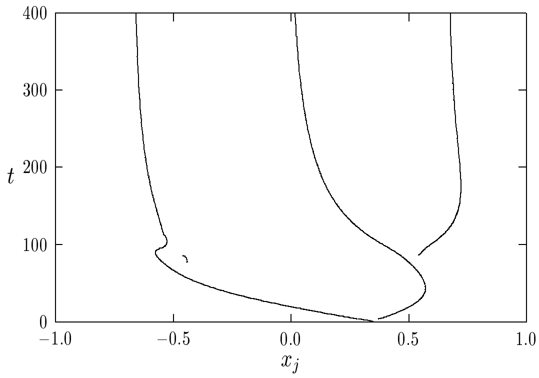

(a) t versus x_j: $A = 3.0$

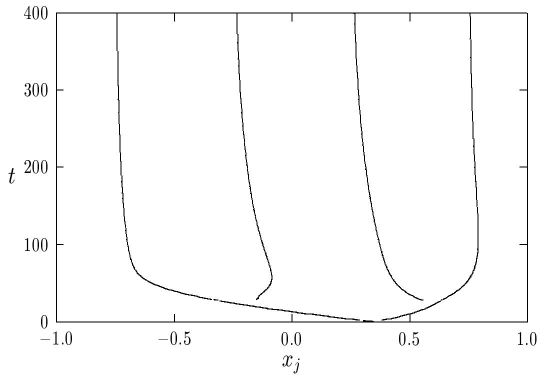

(b) t versus x_j: $A = 4.0$

Figure 17: Experiment 6: t versus x_j for the parameter values $\varepsilon = 0.02$, $k = 1$, $D = 0.75$, $\tau = 2.0$, and with an initial spike at $x_0(0) = 0.35$. Left figure: $A = 3.0$. Right figure: $A = 4.0$.

Experiment 7: In the next four experiments, we examine instabilities that occur when τ is asymptotically large. In this example, we take a one-spike solution as initial data. The parameter values are $D = 0.25$, $A = 1.35$, $\varepsilon = 0.01$, and $k = 1$. For these values, we calculate $B = 1.301$ and $\alpha = 1.366$ from Fig. 6. From the data used to generate Fig. 11(a), we use (6.9b) to estimate that a Hopf bifurcation of the spike profile occurs when $\tau = \tau_H = 230.0$. In addition, from (5.42), we calculate that a Hopf bifurcation in the spike location occurs when $\tau = \tau_{TW} = 55$. In Fig. 18(a) we show an oscillatory instability in the location of the spike for $\tau > \tau_{TW}$. The initial condition was taken to be a spike centered at $x_0(0) = 0.05$. In Fig. 18(b) we show an oscillatory instability of the spike amplitude for a spike that is initially centered at the origin. In this figure, v_m denotes the maximum value of $v(x,t)$.
Experiment 8: Next, we consider instabilities of a two-spike solution when $D = 0.1$, $A = 1.4$, $\varepsilon = 0.01$, and $k = 2$. For these values, we calculate $B = 1.286$ and $\alpha = 1.278$ from Fig. 6. From (6.9b) and Fig. 11(a), we estimate that a Hopf bifurcation of the spike profile occurs when $\tau = \tau_H = 94$. From (5.42), we predict that a Hopf bifurcation in the spike locations occurs when $\tau = \tau_{TW} = 39$.

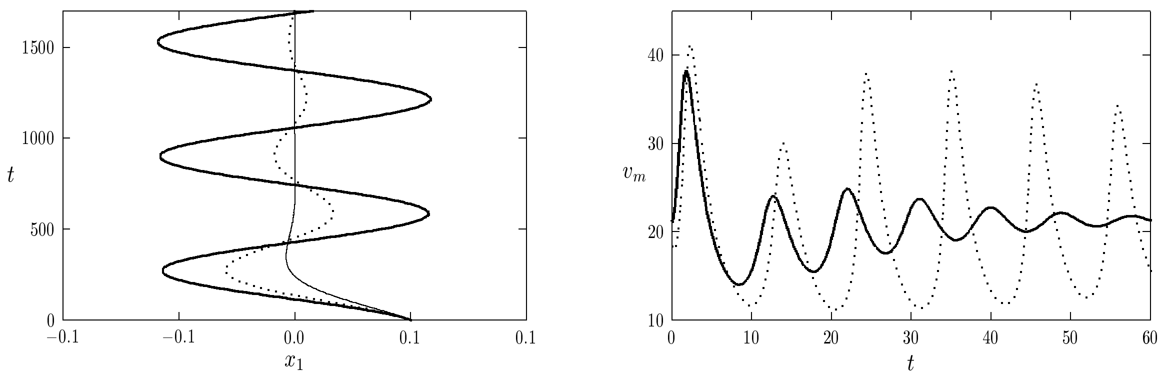

(a) t versus x_1

(b) v_m versus t

Figure 18: Experiment 7: Here $D = 0.25$, $A = 1.35$, $\varepsilon = 0.01$, and $k = 1$. Left figure: t versus x_1 for $\tau = 52$ (solid curve), $\tau = 65$ (dashed curve), and $\tau = 71$ (heavy solid curve). Right figure: v_m versus t for $\tau = 220$ (heavy solid curve) and $\tau = 235$ (dashed curve).

In Fig. 19(a) we show an oscillatory instability in the location of the spikes for $\tau > \tau_{TW}$. Although the spikes are initially located at $x_1(0) = -0.45$ and $x_2(0) = 0.5$, we see from Fig. 19(a) that the instability eventually become a breathing-type instability as predicted by Conjecture 5.6. In Fig. 18(b) we show an oscillatory instability of the spike amplitudes v_m when the spikes are located initially at $x_1(0) = -x_2(0) = 0.5$. Although we have given an asynchronous initial perturbation in the spike amplitudes, the amplitudes are found to quickly synchronize as t increases.

Experiment 9: Next, we take the parameter values $D = 0.25$, $A = 1.35$, $\varepsilon = 0.015$, and $k = 2$. For these values, we calculate $B = 1.286$ and $\alpha = 1.278$ from Fig. 6. From (6.9b) we estimate that $\tau_H = 102$. From (5.42), we predict that $\tau_{TW} = 99.0$ for a two-spike equilibrium solution and $\tau_{TW} = 66.9$ for a one-spike equilibrium solution. Therefore, the thresholds for instabilities with respect to the large and small eigenvalues are very close. We take the parameter value $\tau = 90$ which is near these instability thresholds. The spikes are initially located at $x_1(0) = -0.45$ and $x_2(0) = 0.5$. In Fig. 20(a) we plot the trajectories of the spikes, and in Fig. 20(b) we plot the spike amplitudes $v_{mj} \equiv v(x_j, t)$, where $x_j(t)$ is a local maximum of v. The second spike is annihilated as a result of oscillations of the spike amplitudes. The remaining spike then travels to the right and exits the domain at $t \approx 240$. Notice that since τ exceeds the drift stability threshold for a one-spike solution the final

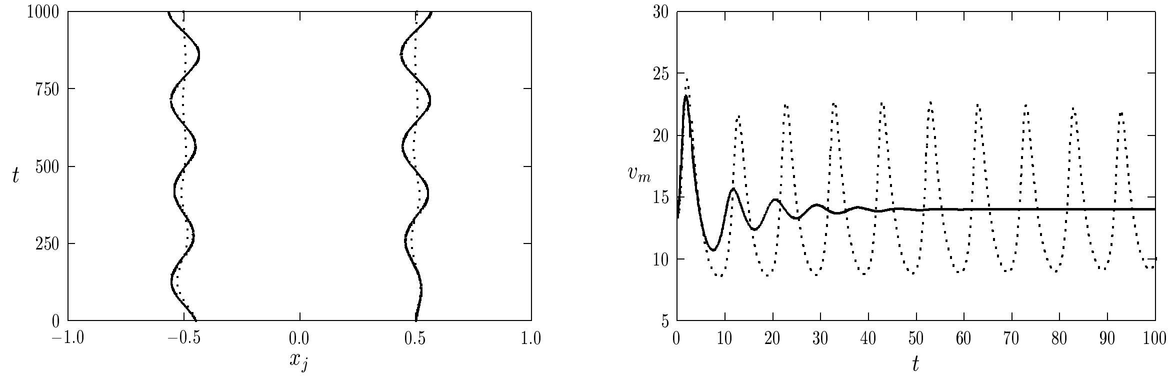

(a) t versus x_j

(b) v_m versus t

Figure 19: Experiment 8: Here $D = 0.1$, $A = 1.4$, $\varepsilon = 0.01$, and $k = 2$. Left figure: t versus x_j for $\tau = 55$ (heavy solid curve) and $\tau = 35$ (dashed curve). Right figure: v_m versus t for $\tau = 85$ (heavy solid curve) and $\tau = 105$ (dashed curve).

equilibrium state should not a be one-spike solution centered at the origin.

Experiment 10: The parameter values are $D = 0.04$, $A = 1.5$, $\varepsilon = 0.0077$, and $k = 1$. The initial condition is taken to be a spike centered at the origin. For this example, we calculate from (3.28) that $A_{p2} = 1.365$ and $A_{p4} = 1.588$. Therefore, for $\tau \ll O(\varepsilon^{-1})$, Conjecture 6.1 predicts a four-spike final equilibrium state. In the dashed curve in the t versus x_j plot of Fig. 21(a) this is indeed observed for the parameter value $\tau = 6.76$. However, for $\tau = 30$, we see from Fig. 21(a) that the solution appears to be a time-periodic two-spike state. For the intermediate value $\tau = 20$, we observe a time-periodic two-spike state that every half-period undergoes a brief splitting process before collapsing back to a two-spike solution. For this example, $\tau_{TW} = 35$ for a four-spike equilibrium solution, and $\tau_H = 64$.

Experiment 11: In this last example we consider drift instabilities of a three-spike equilibrium solution when $D = 0.1$, $A = 1.6$, $\varepsilon = 0.01$, and $k = 3$. From (5.42), we predict that a Hopf bifurcation in the spike locations occurs when $\tau = \tau_{TW} = 49.3$. From (6.9b), a Hopf bifurcation in the spike amplitudes should occur when $\tau = \tau_H = 94.5$. In Fig. 21(b) we show an oscillatory instability in the location of the spikes for $\tau = 75$. Although the initial locations of the spikes are chosen to be $x_1(0) = -0.45$, $x_2(0) = 0.0$, and $x_3(0) = 0.50$, we see from Fig. 21(b) that the instability eventually becomes a breathing-type instability as predicted by Conjecture 5.6.

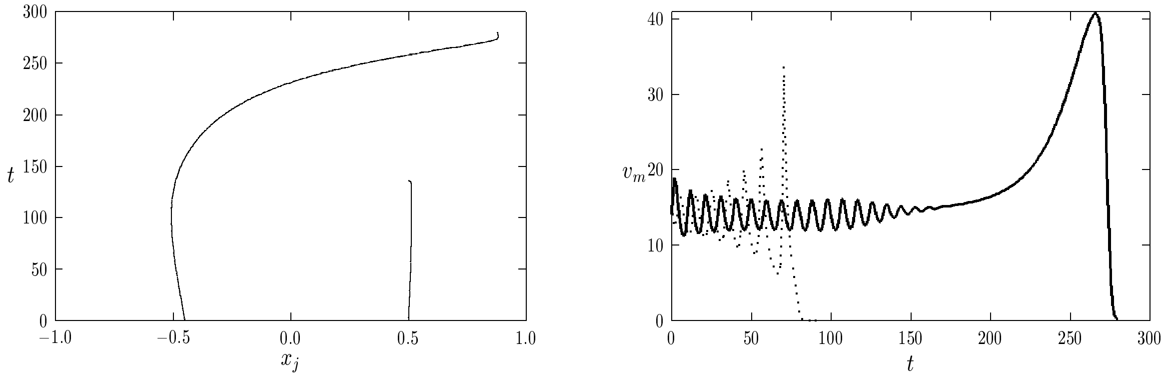

(a) t versus x_j

(b) v_m versus t

Figure 20: Experiment 9: Here $D = 0.25$, $A = 1.35$, $\varepsilon = 0.015$, $k = 2$, and $\tau = 90$. Left figure: t versus x_j. Right figure: v_{m1} versus t (heavy solid curve) and v_{m2} versus t (dashed curve).

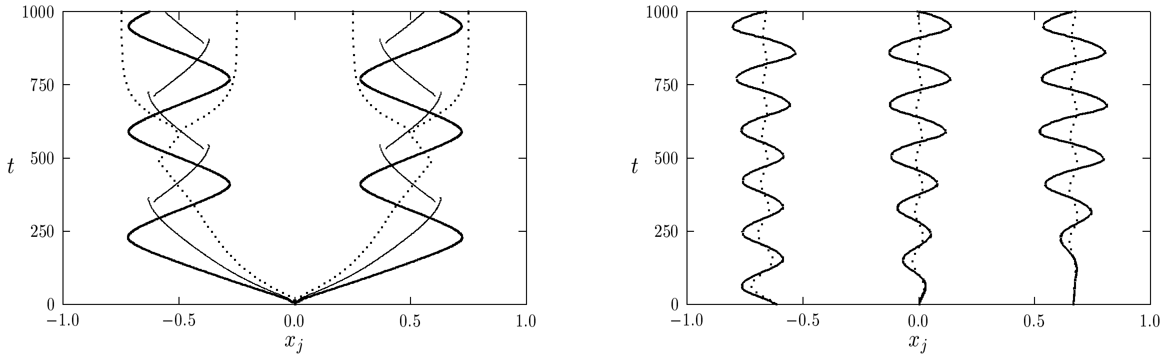

(a) t versus x_j

(b) t versus x_j

Figure 21: Left figure: Experiment 10: Here $D = 0.04$, $A = 1.5$, $k = 1$, $\varepsilon = 0.0077$, with $\tau = 6.76$ (dashed curve), $\tau = 20.0$ (solid curve), and $\tau = 30.0$ (heavy solid curve). Right figure: Experiment 11: Here $D = 0.1$, $A = 1.6$, $k = 3$, $\varepsilon = 0.01$, with $\tau = 45$ (dashed curve) and $\tau = 75$ (heavy solid curve).

8 Discussion

In this section we discuss a few pulse-splitting numerical simulations that have appeared in the literature and that are relevant to our semi-strong pulse interaction regime. We also list some open problems and give a few areas for further research.

A common dimensionless formulation of the Gray-Scott model (cf. [5], [6], [7], [9], [36], and [37]) takes the form

$$V_T = \mathcal{D} V_{XX} - B_d V + U V^2 \,, \qquad 0 < X < L \,, \quad T > 0 \,, \tag{8.1a}$$

$$U_T = U_{XX} + A_d (1 - U) - U V^2 \,, \qquad 0 < X < L \,, \quad T > 0 \,, \tag{8.1b}$$

with $U_X = V_X = 0$ at $X = 0, L$. In terms of our dimensionless groupings of (1.3), we have

$$D \equiv \frac{4}{A_d L^2} \,, \qquad \varepsilon^2 \equiv \frac{4\mathcal{D}}{B_d L^2} \,, \qquad \tau \equiv \frac{B_p}{A_p} \,, \qquad A \equiv \frac{\sqrt{A_d}}{B_d} \,. \tag{8.2}$$

Pulse-splitting for (8.1) was computed numerically in [6] (see Fig. 4 of [6]) for the parameter values $A_d = .01$, $B_d = 0.0474$, $\mathcal{D} = 0.01$, and $L = 100$. The final equilibrium state was observed to have eight spikes, although no theoretical explanation of the final state was given in [6]. In terms of our variables, we use (8.2) to get $\varepsilon = .00918$, $D = 0.04$, $A = 2.109$, and $\tau = 4.74$. This is the first example of Experiment 5 of §6.2, where we correctly predicted the eight-spike equilibrium state. In Fig. 2b of [5] a four-spike final state was computed for $A_d = .01$, $B_d = 0.0674$, $\mathcal{D} = 0.01$, and $L = 100$. In terms of our variables, we get $\varepsilon = .0077$, $D = 0.04$, $A = 1.483$, and $\tau = 6.74$. This is the second example of Experiment 5. Pulse-splitting in the semi-strong interaction regime has also been observed in terms of the original formulation of the Gray-Scott model in (1.1) (see [36] and [3]). For the parameter values $D_u = 1.0$, $D_v = 0.01$, $F = 0.02$, $k = 0.059$, and $L = 60$, the final equilibrium state in Fig. 4.1b of [3] was observed to have eight spikes (see also [36]), although again no theoretical explanation was given to predict the final state. For these values, we get from (1.4) and (3.28) that $\varepsilon = 0.0119$, $D = 0.0555$, $A = 1.7901$, $\tau = 1.339 = O(1)$, $A_{p4} = 1.7135$, and $A_{p8} = 2.7725$. Since $A_{p4} < A < A_{p8}$, and τ is below the instability threshold, the Conjecture 6.1 correctly predicts an eight-spike final equilibrium state.

There are many open problems related to pulse-splitting that await a rigorous proof. Two central problems are to prove rigorously the shape of the $B = B(\gamma)$ curve in Fig. 2(a), and to prove the formal results in Propositions 3.2, 4.1, and 4.2, that give the saddle-node bifurcation values A_{pk} and the qualitative properties of solutions along the two extremes of the $B(\gamma)$ curve. Another important open problem is to give a rigorous treatment of the stability of the primary and secondary solution branches with respect to both drift instabilities and instabilities associated with the large eigenvalues.

Other areas where further research is needed is to characterize the dynamics of quasi-equilibrium spike patterns for (1.3) in the pulse-splitting regime, and to predict the times and locations where splitting events occur. In particular, a theoretical explanation of Experiments 6, 9 and 10 would be interesting. For semi-strong spike interactions, the dynamics of a two-spike evolution in the intermediate parameter regime were studied in [5] and [6]. Spike dynamics for the Gierer-Meinhardt model in the semi-strong regime were studied in [17]. For the weak interaction regime of [32], where both diffusivities are small and of the same order, spike dynamics was studied in [10] and [11]. Secondly, it would be interesting to study the stability of stripe and ring patterns in the two dimensional Gray-Scott model with respect to both zig-zag instabilities associated with the small eigenvalues, and breakup instabilities of stripes into spots, which result from large eigenvalue instabilities. Some work in this direction is given in [21], [25], and [20].

Acknowledgements

T. K. was supported by a PGS-B graduate scholarship from NSERC (Canada). M. J. W. thanks the grant support of NSERC, and the IMS of the Chinese University of Hong Kong where most of this paper was written. J. W. thanks the support of RGC of Hong Kong and a direct grant from CUHK. M. J. W. is most grateful to the University of Washington Applied Math group for the generous use of their computer facilities.

References

[1] E. Anderson et al. *LAPACK User's Guide: Third Edition*, SIAM Publications (1999).

[2] U. Ascher, R. Christiansen, R. Russell, *Collocation Software for Boundary Value ODE's*, Math. Comp., **33**, (1979), pp. 659-679.

[3] E. J. Crampin, P. K. Maini, *Reaction-Diffusion Models for Biological Pattern Formation*, Methods and Appl. of Analysis, **8**, No. 2, (2001), pp. 415-428.

[4] M. Del Pino, M. Kowalczyk, X. Chen, *The Gierer Meinhardt System: The Breaking of Homoclinics and Multi-Bump Ground States*, Commun. Contemp. Math., **3**, No. 3, (2001), pp. 419-439.

[5] A. Doelman, W. Eckhaus, T. J. Kaper, *Slowly Modulated Two-Pulse Solutions in the Gray-Scott Model I: Asymptotic Construction and Stability*, SIAM J. Appl. Math., **61**, No. 3, (2000), pp. 1080-1102.

[6] A. Doelman, W. Eckhaus, T. J. Kaper, *Slowly Modulated Two-Pulse Solutions in the Gray-Scott Model II: Geometric Theory, Bifurcations, and Splitting Dynamics*, SIAM J. Appl. Math., **61**, No. 6, (2000), pp. 2036-2061.

[7] A. Doelman, R. A. Gardner, T. J. Kaper, *Stability Analysis of Singular Patterns in the 1D Gray-Scott Model: A Matched Asymptotics Approach*, Physica D, **122**, No. 1-4, (1998), pp. 1-36.

[8] A. Doelman, R. A. Gardner, T. Kaper, *A Stability Index Analysis of 1-D Patterns of the Gray Scott Model*, Memoirs of the AMS, **155**, No. 737, (2002).

[9] A. Doelman, T. J. Kaper, P. Zegeling, *Pattern Formation in the One-Dimensional Gray-Scott Model*, Nonlinearity, **10**, No. 2, (1997), pp. 523-563.

[10] S. Ei, Y. Nishiura, K. Ueda, 2^n *Splitting or Edge Splitting?: A Manner of Splitting in Dissipative Systems*, Japan. J. Indust. Appl. Math., **18**, (2001), pp. 181-205.

[11] S. Ei, *The Motion of Weakly Interacting Pulses in Reaction-Diffusion Systems*, J. Dynam. Differential Equations, **14**, No. 1, (2002), pp. 85-137.

[12] T. Erneux, E. L. Reiss, L. J. Holden, M. Georgiou, *Slow Passage Through Bifurcation and Limit Points. Asymptotic Theory and Applications*, Dynamic Bifurcations (Luminy 1990), Lecture Notes in Math., **1493**, Springer, Berlin, (1991), pp. 14-28.

[13] A. Gierer, H. Meinhardt, *A Theory of Biological Pattern Formation*, Kybernetik, **12**, (1972), pp. 30–39.

[14] G. Goldsztein, F. Broner, S. H. Strogatz, *Dynamical Hysteresis Without Static Hysteresis: Scaling Laws and Asymptotic Expansions*, SIAM J. Appl. Math., **57**, No. 4, (1997), pp. 1163-1187.

[15] P. Gray, S. K. Scott, *Autocatalytic Reactions in the Isothermal, Continuous Stirred Tank Reactor: Oscillations and Instabilities in the System* $A + 2B \to 3B,\ B \to C$, Chem. Eng. Sci. **39**, (1984), pp. 1087-1097.

[16] T. Ikeda, Y. Nishiura, *Pattern Selection for Two Breathers*, SIAM J. Appl. Math., **54**, No. 1, (1994), pp. 195-230.

[17] D. Iron, M. J. Ward, *The Dynamics of Multi-Spike Solutions to the One-Dimensional Gierer-Meinhardt Model*, SIAM J. Appl. Math., **62**, No. 6, (2002), pp. 1924-1951.

[18] D. Iron, M. J. Ward, J. Wei, *The Stability of Spike Solutions to the One-Dimensional Gierer-Meinhardt Model*, Physica D, **150**, No. 1-2, (2001), pp. 25-62.

[19] T. Kolokolnikov, M. Ward, J. Wei, *The Stability of Spike Equilibria in the One-Dimensional Gray-Scott Model: The Low Feed-Rate Regime*, submitted, AMS Monographs, (2003).

[20] T. Kolokolnikov, M. Ward, J. Wei, *Zigzag and Breakup Instabilities of Stripes and Rings in the Two Dimensional Gray-Scott Model*, to be submitted, Journ. Nonlinear Science, (2003).

[21] T. Kolokolnikov, J. Wei, *On Ring-Like Solutions for the Gray-Scott Model: Existence, Instability, and Self-Replicating Regimes*, submitted, Nonlinearity, (2003).

[22] K. J. Lee, W. D. McCormick, J. E. Pearson, H. L. Swinney, *Experimental Observation of Self-Replicating Spots in a Reaction-Diffusion System*, Nature, **369**, (1994), pp. 215-218.

[23] K. J. Lee, H. L. Swinney, *Lamellar Structures and Self-Replicating Spots in a Reaction-Diffusion System*, Phys. Rev. E., **51**, (1995), pp. 1899-1915.

[24] M. Mimura, N. Nishiura, *Layer Oscillations in Reaction Diffusion Systems*, SIAM J. Appl. Math., **49**, No. 2, (1989), pp. 481-514.

[25] D. Morgan, T. Kaper, *Axisymmetric Ring Solutions of the Gray-Scott Model and Their Destabilization into Spots*, submitted, Physica D, (2003).

[26] C. Muratov, V. V. Osipov, *Traveling Spike Auto-Solitons in the Gray-Scott Model*, Physica D, **155**, No. 1-2, (2001), pp. 112-131.

[27] C. Muratov, V. V. Osipov, *Stability of the Static Spike Autosolitons in the Gray-Scott Model*, SIAM J. Appl. Math., **62**, No. 5, (2002), pp. 1463-1487.

[28] C. Muratov, V. V. Osipov, *Static Spike Autosolitons in the Gray-Scott Model*, J. Phys. A: Math Gen. **33**, (2000), pp. 8893-8916.

[29] NAG Fortran library Mark 17, routine D03PCF, Numerical Algorithms Group Ltd., Oxford, United Kingdom (1995).

[30] Y. Nishiura, *Global Bifurcational Approach to the Onset of Spatio-Temporal Chaos in Reaction-Diffusion Systems*, Methods and Appl. of Analysis, **8**, No. 2, (2001), pp. 321-332.

[31] Y. Nishiura, T. Teramoto, K. Ueda, *Scattering and Separators in Dissipative Systems*, Phys. Rev. E., **67**, No. 5, 56210, (2003).

[32] Y. Nishiura, D. Ueyama, *A Skeleton Structure of Self-Replicating Dynamics*, Physica D, **130**, No. 1-2, (1999), pp. 73-104.

[33] Y. Nishiura, D. Ueyama, *Spatio-Temporal Chaos for the Gray-Scott Model*, Physica D, **150**, No. 3-4, (2001), pp. 137-162.

[34] J. E. Pearson, *Complex Patterns in a Simple System*, Science, **216**, (1993), pp. 189-192.

[35] V. Petrov, S. K. Scott, K. Showalter, *Excitability, Wave Reflection, and Wave Splitting in a Cubic Autocatalysis Reaction-Diffusion System*, Phil. Trans. Roy. Soc. London, Series A, **347**, (1994), pp. 631-642.

[36] W. N. Reynolds, S. Ponce-Dawson, J. E. Pearson, *Dynamics of Self-Replicating Patterns in Reaction-Diffusion Systems*, Phys. Rev. Lett., **72**, (1994), pp. 2797-2800.

[37] W. N. Reynolds, S. Ponce-Dawson, J. E. Pearson, *Dynamics of Self-Replicating Spots in Reaction-Diffusion Systems*, Phys. Rev. E, **56**, No. 1, (1997), pp. 185-198.

[38] D. Ueyama, *Dynamics of Self-Replicating Patterns in the One-Dimensional Gray-Scott Model*, Hokkaido Math J., **28**, No. 1, (1999), pp. 175-210.

[39] M. J. Ward, J. Wei, *Hopf Bifurcations and Oscillatory Instabilities of Spike Solutions for the One-Dimensional Gierer-Meinhardt Model*, Journal of Nonlinear Science, **13**, No. 2, (2003), pp. 209-264.